Master's thesis

NTNU
Norwegian University of Science and Technology
Faculty of Medicine and Health Sciences
Department of Clinical and Molecular Medicine

Ana Beatriz Núñez Nescolarde

Use of CRISPR/Cas9-Mediated Genome Editing in Human Induced Pluripotent Stem Cells to Study Oxidative Base Lesion Repair in Cerebral Organoids

Master's thesis in Molecular Medicine

Supervisor: Katja Scheffler

June 2020

NTNU
Norwegian University of Science and Technology

Ana Beatriz Núñez Nescolarde

Use of CRISPR/Cas9-Mediated Genome Editing in Human Induced Pluripotent Stem Cells to Study Oxidative Base Lesion Repair in Cerebral Organoids

Master's thesis in Molecular Medicine
Supervisor: Katja Scheffler
June 2020

Norwegian University of Science and Technology
Faculty of Medicine and Health Sciences
Department of Clinical and Molecular Medicine

NTNU
Norwegian University of
Science and Technology

Acknowledgements

I wish to express my deepest gratitude to my supervisor, **Associate Professor Katja Scheffler**, who is not only an outstanding and passionate professional but also a very determined and smart woman. The way she leads her group, ensuring quality time for each of her students is beyond stipulated. The freedom, support and trust she gave me this year helped me grow both academically and personally. I can only encourage other students to be under her tutelage.

I also want to recognize the invaluable assistance of my co-supervisor **Researcher Wei Wang**. Thanks to him I found myself trap in the amazing world of stem cells and organoids; always with the kindest words, optimism, and a lot of experience Wei convincingly guided and encouraged me to do it right when the road got tough.

At the very beginning of this master's thesis, Wei and Katja sat down with me and warned me about the difficulties of this project. I did not understand what they meant. However, a year and a half later, I can only thank them. I started to learn what f-r-u-s-t-r-a-t-i-o-n means: months of work, gone in one day. But you know what they say: "this is science". Therefore, as a student I want to express my admiration to the scientific community, who despite being surrounded by darkness is enfolded in light.

A huge thanks to the **Senior Engineer Per Arne Aas**, who designed the CRISPR/Cas9 plasmids used in this project and has the best tricks for a successful PCR and a good-looking agarose gel. Also, I am indebted to the **Professor Xiao-Bing Zhang** from Loma Linda University in California for facilitating us the crucial BCL-XL plasmid. All my gratitude to the **Senior Engineer Nina-Beate Liabakk**, for the innumerable amount of times she dedicated to help me with the FACS.

Moreover, I would like to thank **Alix**, **Andres**, **Erland**, **Ezgi**, **Konika**, **Lene**, **Milena, Nina**, **Teri**, **Tobias** and **Vishnu**; colleagues that are now friends and gave me the best of their advices and support throughout this year. Trondheim is not as cold and not as dark with you guys.

Lastly and most important, I want to thank my family: my parents **Lexa and Paco** and my partner **Lindsay.** Your unconditional love and support are the reasons that keep me going and make me be the best version of myself. Mum and dad, I have seen you doing so many sacrifices for me, that I do not think there is a way I can pay back all that love you showed me. Thank you. And thanks also to my partner, who despite being far away managed to find a way to be closer than ever.

Abstract

The role of DNA glycosylase OGG1 beyond the base excision repair (BER) pathway involves regulation of brain development and function. However, the molecular mechanisms remain to be unravelled. Here, we describe a reliable method to obtain *OGG1* deficient human induced pluripotent stem cells (hiPSCs) via CRISPR/Cas9 technology. We observed that electroporation and flow cytometry led to massive death on hiPSCs. However, transient overexpression of BCL-XL and the subsequent treatment with Navitoclax enhanced cell survival and transfection efficacy after electroporation using Human Stem Cell Nucleofactor® Kit 1. Moreover, culture medium supplemented with RevitaCell further improved cell viability after flow cytometry.

It was shown that cerebral organoids recapitulate the first trimester of human brain development. Interestingly, *OGG1* expression increased as the organoid development progressed. Our results on gene expression pattern from three different stages of cerebral organoid development, were consistent with previous studies, suggesting that organoids are a reliable *in vitro model.*

Taken together, these methods can be applied for the generation of genetically modified cerebral organoids.

Table of Contents

List of Figures

List of Tables

Abbreviations

AP	Apurinic/apyrimidinic
ANOVA	Analysis of variance
APE1	AP endonuclease 1
BER	Base excision repair
BSA	Bovine serum albumin
BHT	Butylated Hydroxy Toluene
5caC	5-carboxylcytosine
CHD4	DNA-binding protein 4
CNS	Central nervous system
CRISPR	Clustered regularly interspaced short palindromic repeats
DEGs	Differentially expressed genes
DFO	Deferoxamine
DNMTs	DNA methyltransferases
DSBs	Double-strand breaks
EBs	Embryoid bodies
EHMT2	Euchromatic histone lysine methyl-transferase 2
ESR1	Estrogen receptor 1
EZH2	Enhancer of zeste 2 polycomb repressive complex 2 subunit
FACS	Fluorescence-activated cell sorting
FBS	Fetal bovine serum
5fC	5-formyl
FGF2	Fibroblast growth factor 2
GFP	Green fluorescent protein
HIER	Heat induced epitope retrieval
IPA	Ingenuity Pathway Analysis
iPSC	Induced pluripotent stem cells
iROCK	Inhibitor of Rho-associated, coiled-coil containing protein kinase
LIG1	DNA ligase 1
LIG3	DNA ligase 3
LC-MS	Liquid chromatography-mass spectrometry
POLβ	DNA polymerase β
EBs	Embryoid bodies
FEN1	Flap endonuclease 1 (FEN1)
HDR	Homology-directed repair
HIER	Heat induced epitope retrieval
hiPSCs	human induced pluripotent stem cells
5hmC	5-hydroxymethyl
5mC	5-methylcytosine
NHEJ	Nonhomologous end-joining
NOX	NADPH oxidases
8-oxoG	8-oxoguanine
PAM	Protospacer adjacent motif
PCNA	Proliferating cell nuclear antigen
PDGF	Platelet-derived growth factor
PNKP	Polynucleotide kinase phosphatase
ROS	Reactive oxygen species
gRNA	Guide RNA
SSBs	Single strand breaks
SSBR	Single-strand break repair
TALEN	Transcription activation-like effector nuclease
TDP1	Ttyrosyl DNA phosphodiesterase 1
Tet	Ten-eleven translocation
XRCC1	X-ray repair cross-complementing protein 1

1. Introduction

1.1. Reactive Oxygen Species and Brain Function

The human brain accounts for more than 20% of the energy consumption of the body (1). Neurons carry a high number of mitochondria, which reduces oxygen and releases ATP at a high rate, to support the continuous transmission of neuronal signals and prevent neurodegeneration (2, 3). However, reactive oxygen species (ROS) are produced as byproducts of this reaction (4). The toxicity of oxygen is explained by its capacity to produce free radical and non-radicals species, such as superoxide, hydrogen peroxide and the hydroxyl radical; that can oxidise and damage essential macromolecules within the cell (5). A phenomenon called oxidative stress appears when the production of ROS exceeds the natural antioxidant scavenging ability of the cell (6). Therefore, good antioxidant mechanisms would be expected from such a considerable oxygen consumer as it is the brain. However, when compared to other organs, the brain is more susceptible to oxidative stress, and this cannot be explained by the mere assumption that oxygen is good whilst its adventitious reactive progeny are bad (7). Instead, ROS has been associated with pivotal biological functions after the discovery of the membrane bound NADPH oxidases (NOX), whose main roles are the production of these reactive species (8). Chang et al. revealed that hydrogen peroxide and superoxide anion produced by NOX maintain neural progenitor cells in the hippocampus (9). Role in synaptic plasticity and memory regulation has also been associated with ROS (10). Moreover, a recent study carried out in *Caenorhabditis elegans* showed that transient increase in ROS levels improved redox homeostasis, stress resistance and prolonged lifespan of the animals (11). However, excessive ROS and imbalance in the redox signalling may induce neurodegeneration and ageing (3). Indeed, it is shown that ROS production is higher in Alzheimer's and Parkinson's diseases (12-14). The reliance of the brain in calcium, glutamate excitotoxicity, glucose, microglia,

and the generation of hydrogen peroxide by endogenous amine-based neurotransmitters, can cause oxidative stress in the brain (15).

It has been extensively reported that ROS oxidise and damage proteins, lipids and nucleic acids (16). While oxidized proteins, lipids and RNA can be degraded and recycled, the DNA has to be repaired to maintain genomic stability (17).

1.2. Base Excision Repair Mechanism

Each human cell encounters approximately 70,000 lesions per day. The most common DNA lesions derived from oxidative damage are apurinic/apyrimidinic (AP) sites, followed by DNA single strand breaks (SSBs) and base lesions (18). Damage in DNA bases can lead to AP sites. The most frequently oxidized DNA base is guanine at carbon C4, C5 and C8 position, with 8-oxoguanine (8-oxoG) being the most recurring (6). Every day in the cell, up to 10,000 8-oxoG lesions with highly mutagenic properties are generated (19). 8-oxoG can pair both with cytosine and adenine, resulting in G to T transversion (20). Indeed, it is accumulated in the nuclear and mitochondrial DNA during aging and play an important role in the development of cancer (21).

Oxidized DNA base lesions are mainly repaired by the base excision repair/single-strand break repair (BER/SSBR) pathways. In BER pathway, base lesions can be recognized by several DNA glycosylases, which are then classified into two different groups: monofunctional and bifunctional DNA glycosylases (22). Monofunctional glycosylases cleave the C1′-*N*-glycosidic bond generating AP sites, whilst bifunctional DNA glycosylases possess both glycosylase activity but also AP lyase activity that creates SSB by β-elimination or β/δ-elimination reaction (23). The monofunctional DNA glycosylase MUTYH and the bifunctional DNA glycosylase OGG1, cooperate to prevent mutations caused by 8-oxoG (Figure 1) (22, 24). BER pathway converges

with the SSB repair pathway after the AP lyase activity of the bifunctional DNA glycosylases or the cleavage of the phosphodiester bond by the AP endonuclease 1 (APE1) following a monofunctional DNA glycosylase (25). SSB end processors such as DNA polymerase β (POLβ), APE1, Aprataxin, tyrosyl DNA phosphodiesterase 1 (TDP1) and polynucleotide kinase phosphatase (PNKP), cooperate to provide the free 3′ hydroxyl group needed for the polymerases to insert nucleotides. The resulting gap will be processed either by the short-patch or long-patch BER depending on several factors, for instance, the cell cycle phase. In the short-patch BER, POLβ and DNA ligase 3 (LIG3), insert and seal one nucleotide respectively, and the process is organized by X-ray repair cross-complementing protein 1 (XRCC1). In the long-patch BER, a longer fragment of DNA is removed, and in this case, the process is orchestrated by the proliferating cell nuclear antigen (PCNA). The POLδ/ε synthetize the new strand while creating a flap, which in turn will be removed by the flap endonuclease 1 (FEN1) before ligation with LIG1 (25). The process described above is applicable to nuclear BER. Although the enzymatic process of BER proteins on mitochondrial DNA is similar, mitochondria differ in the BER complex composition (26).

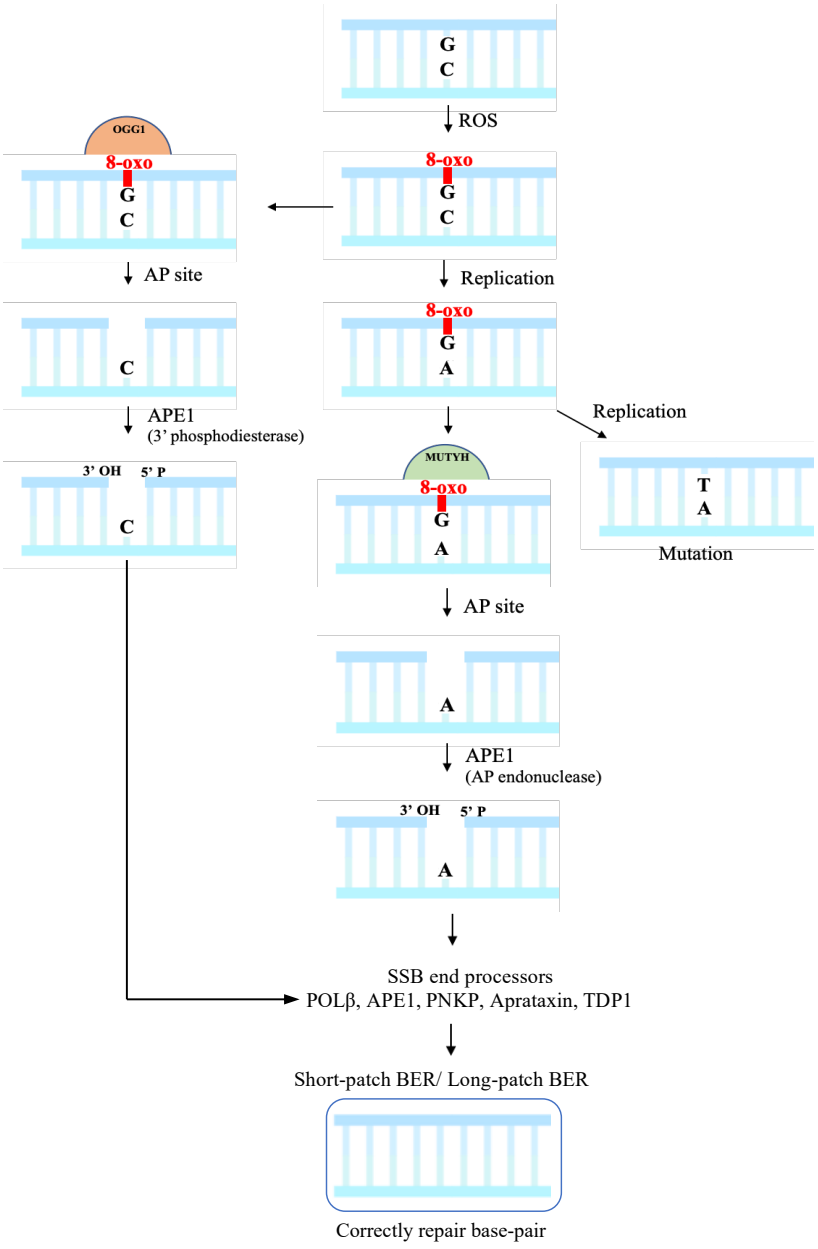

Figure 1. Schematic representation of the base excision repair pathway. Being the predominant DNA repair pathway for small base lesions, BER is initiated by lesion-specific DNA glycosylases. OGG1 removes 8-oxoG from 8-oxoG·C, and MUTYH removes A from 8-oxoG·A, generating apurinic/apyrimidinic sites in the DNA that, afterwards, will be repaired by the short-patch, where only one nucleotide is replaced, or by the long-patch where 2-13 nucleotides are replaced.

1.3. Non-Canonical Function of OGG1

As mentioned in section 1.2, the bifunctional DNA glycosylase OGG1 is the main enzyme for the excision of 8-oxoG. If the lesion is not repaired mutations can arise, increasing the chance of developing cancer. However, due to the redundancy in DNA glycosylases, the correlation between cancer development in humans and mutations in BER genes is very low (27). Experiments carried out in mice, suggested that *Ogg1*$^{-/-}$ *Mutyh*$^{-/-}$ genotype do develop cancer (28). Whereas mice with deletion only in *Ogg1* did not present a mutator phenotype despite the accumulation of 8-oxoG in some tissues (29).

Interestingly, a selective role of 8-oxoG in regulating gene expression via epigenetic changes resulting in transcriptionally active chromatin has been reported (30). 8-oxoG has also been associated with the inhibition of DNA methylation, since the presence of 8-oxoG adjacent to a target cytosine interfered with the function of DNA methyltransferases (DNMTs), favouring non-productive bindings (31). Moreover, DNA glycosylase OGG1 promoted DNA demethylation. 8-oxoG lesions caused by oxidative stress, enhanced recruitment of OGG1, and Zhou and co-workers demonstrated that OGG1 recruited TET1 (Ten-eleven translocation 1) and that the interaction was not DNA dependant (32). TET family proteins oxidize the modified genomic base 5-methylcytosine (5mC) to 5-hydroxymethyl (5hmC), 5-formyl (5fC), and 5-carboxylcytosine (5caC), that in turn can be recognised and excised by the BER pathway (33). In addition, genes that are normally repressed in brain and characterized by high-CpG-density promoters bearing histone H3 trimethylation at K4 and at K27, showed increase in their expression in *Ogg1*$^{-/-}$ and/or *Mutyh*$^{-/-}$ mice, suggesting that the accumulation of 8-oxoG at gene regulatory regions might affect epigenetically and transcriptionally neuronal cells (34).

However, *Ogg1* has not only been associated with the transcriptional activation of certain genes, but it has also been suggested to have a negative regulation in gene expression (35). It is believed that under oxidative stress, OGG1 enhance repressive chromatin conformation and the consequent gene silencing (36). ChIP sequencing pointed to guanine-rich promoter as the primary substrate for OGG1, mainly linked to genes involved in immune response, oxidative stress, signal transduction and cellular homeostasis (37).

Oxidative damage is associated with neurodegeneration and increases with age; therefore, it has been of interest to investigate the role of DNA glycosylases on brain function. Critical functions such as preventing metabolic and oxidative stress are been associated with BER-related OGG1 enzyme in cortical neurons after demonstrating reduced motor function in aged $Ogg1^{-/-}$ mice (38). Nonetheless, other non-canonical roles of OGG1 in the brain have been widely highlighted. To have a better understanding of 8-oxoG dependent DNA glycosylases on hippocampal-dependent learning and memory, 6-months old $Ogg1^{-/-}Mutyh^{-/-}$ mutant mice were examined in a zero maze and water maze test. Interestingly, compared to wild type and single knockout, double knockout mice showed less anxiety and were more active. Memory in $Ogg1^{-/-}Mutyh^{-/-}$ mice was not affected, however, they did show impaired learning. Bjørge and colleagues suggested different roles for DNA glycosylases OGG1 and MUTYH in the regulation of cognition, since OGG1 seemed to have dominant effect on learning, but $Mutyh^{-/-}$ mice did not present any learning impairment (34). Several repressive mechanisms for memory formation in the hippocampus have been reported, for instance, suppression of genes via inhibition of estrogen receptor 1 (ESR1/ERα) signalling (39). Interestingly, ESR1 was identified as an upstream regulator of differentially expressed genes (DEGs) in the hippocampus of mice lacking OGG1 and/or MUTYH, suggesting that the DNA

glycosylases repress Esr1 signalling to support memory formation (34). However, their roles and mechanisms involved in human brain development and function are yet to be unravelled.

1.4. Human Induced Pluripotent Stem Cells

Large parts of the brain and spinal cord can be regenerated in amphibians following amputation. Skin, muscle and bone cells immediate to the amputation site revert into a clump of adult stem cells so-called blastema (40). Stem cells are precursor cells with capacity to self-renew and able to differentiate generating multiple cell types (41). However, in the mammalian adult brain, the capacity of self-repair is minimal due to the low amount of stem cells capable of generating new neurons and the inability of neurons to complete a successful mitosis (16, 42). In a typical differentiated cell, there are molecular mechanisms that ensure maintenance of the pattern in gene expression from one cell generation to the next, continuing with the cell lineage (16). However, in 2006 Shinya Yamanaka demonstrated the possibility of obtaining the so-called induced pluripotent stem cells (iPSC) from already differentiated cells. By transfecting fibroblast with retroviral vectors coexpressing the transcription regulators Oct3/4, Sox2, c-Myc and Klf4, under embryonic stem cells culture conditions, it was possible to obtain cells with morphology and growth properties comparable to embryonic stem cells as well as the expression of pluripotency markers (43). Both embryonic stem cells and iPSCs share the property of dividing indefinitely in culture and are capable forming a chimeric animal when incorporated into a mouse blastocyst. In this animal, Yamanaka's group could visualize by using green fluorescent protein (GFP), that iPSCs contributed to all three germ layer and could differentiate into any tissue of the body (43). Moreover, it was shown that cultured iPSCs could further differentiate to a given desired cell type with the right combination of growth factor in the medium (43).

Multiple studies have been conducted and proved the generation of human induced pluripotent stem cells (hiPSCs) from human somatic cells by ectopic expression of the four transcription factors stated in Yamanaka's first publication, Oct3/4, Sox2, c-Myc and Klf4 (44-46). Indeed, the discovery of iPSCs by Shinya Yamanaka harbours a promising future in research areas that have not been developed yet due to the demand of a human model system (47). For instance, rejection following transplantation of cells or tissue derived from embryonic stem cells is a significant hurdle in clinical research, however, a patient-specific pluripotent stem cell would overcome immune rejection (48).

1.5. Genome Editing in Human Pluripotent Stem Cells

The approach of human induced pluripotent stem cell (hiPSC) reprograming enables the study of disease-causing genetic mutations by comparison of a patient-derived hiPSCs to a healthy subject hiPSCs, by means of differentiating them to the cell type involved in the studied disease (49). The significant variability in the phenotypic characteristics and differentiation propensities of hiPSC from the same donor, have led to the development of *in vitro* approaches that involve a precise and programable genetic modification in a given clone of hiPSCs (50). Custom-engineered endonucleases introduce site-specific double-strand breaks (DSBs) in the genome that are repaired precisely by the homology-directed repair (HDR) or by the error-prone nonhomologous end-joining (NHEJ) (51). This allows to delete an entire sequence of the genome or precise modify nucleotides sequences by the introduction of a DNA donor template (52). The clustered regularly interspaced short palindromic repeats/Cas9 (CRISPR/Cas9) system involves the Cas9 nuclease to create a site-specific DSB in a given target sequence. The specificity for the target sequence is

given by the so-called guide RNAs (gRNAs), harbouring a customized 20 nucleotides that are co-expressed with the Cas9 (53) (Figure 2).

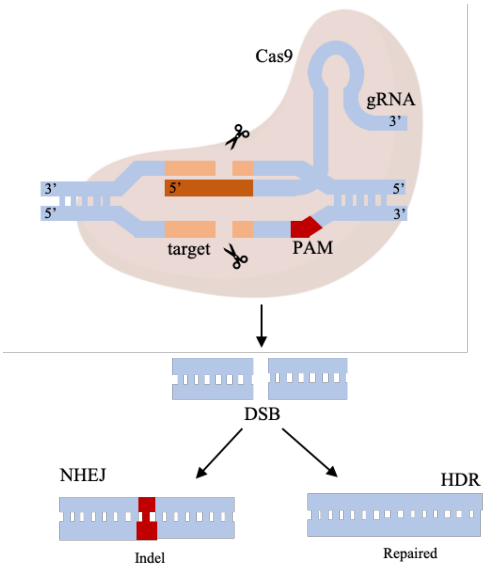

Figure 2. CRISPR/Cas9-mediated genome editing. The state-of-the-art editing technology CRISPR/Cas9 has the basis on the prokaryotic immune system, where evolved as an adaptive surveillance and defense mechanism against foreign genetic elements. Close to the protospacer adjacent motif (PAM) site, customized guide RNA (gRNA) directs the Cas9 protein to genomic targets. After hybridization of 20 nucleotides from the gRNA with one of the DNA strands, Cas9 nuclease introduce a double-stranded break (DBS). Mostly in G2 and S phase of the cell cycle, the genome is repaired by homology-directed repair (HDR). When the homologous DNA is absent, the break is repaired by the error-prone nonhomologous end-joining (NHEJ).

It has been proven that the efficiency in the generation of gene knockout by means of the NHEJ or the HDR-mediated gene editing in hiPSC lines is better using CRISPR/Cas9 than other methods, such as the transcription activation-like effector nuclease (TALEN) (54, 55). However, the CRISPR/Cas9 system is limited to loci harbouring a protospacer adjacent motifs (PAMs). Different Cas9 orthologs require a particular PAM to form a complex with the gRNA-Cas9 (52). In the human genome the PAM motif NGG is found, on average, every 8-12 base pairs (56), therefore this could jeopardize specificity by limiting the CRISPR/Cas9 strategy to NGG-proximal sequences.

1.6. Generation of Cerebral Organoids from Human Induced Pluripotent Stem Cells

In 2014, Lancaster et al. published a revolutionary protocol for the generation of hiPSCs-derived *in vitro* 3D brain tissue, called cerebral organoids (57). HiPSCs can be cultured indefinitely as a monolayer in plates, however, they also harbour the potential to form aggregates in suspension culture, known as embryoid bodies (EBs), and the subsequent differentiation to diverse tissues solely by the addition of specific factors. For instance, it is possible to produce neurons if retinoic acid is included to the medium; whereas, the addition of fibroblast growth factor 2 (FGF2), epidermal growth factor and platelet-derived growth factor (PDGF), promote the formation of astrocytes and oligodendrocytes (16).

In humans, the embryonic period comprises from conception until the eighth gestation week, a period when the rudimentary structures of the brain and the major compartments of the central nervous systems (CNS) are established. In the third week, the three germ layers that give rise to all the structures, including the CNS, are formed. The mesodermal stem cell layer generates the muscles and bones; the endodermal stem cell layer, the respiratory tract and the gut; and cells from the epidermal layer differentiates into the epidermal ectodermal stem cells and neuroectodermal stem cells. Nails, skin, and sweat glands developed from the epidermal ectodermal stem cells, while the neuroectodermal stem cells, also known as neural progenitor cells, give rise to the CNS (58, 59). Similar to human embryonic development, hiPSCs can develop all germ layers when stimulated *in vitro.* Within the EBs, hiPSCs can from an uniform neural ectoderm formation along the surface of the EBs and non-neural inner mesodermal tissue (60).

The brain development continues with the formation of the neural tube during the third week. The neural tube extends along the anterior-posterior axis of the developing embryo. The neural

progenitor cells from the anterior region develop the forebrain and midbrain, whilst the hindbrain and spinal column are formed form the neural progenitor cells of the more caudal region. Around day 42 in the embryonic period, neurons start to be produced. Neural progenitor cells transition to the so-called radial glia which shift their mode of division from symmetrical to asymmetrical, producing two different types of cells (58, 61). Neuron production is carried out in the proliferative regions of the ventricular zone, and shortly after, they migrate to their proper location within the brain guided by the basal radial glia (62). Upon reaching their target locations, neurons begin to differentiate and mature, producing neurotransmitter and neurotrophic factors, and extending axons and dendrites to form a rudimentary neural network (63). The early fetal period, which begins with the ninth gestational week, is critical in the development of the neocortex (58). After being produced, neurons migrate and position themselves in an inside-out manner to form the six-layered neocortical mantel (47).

Established protocols from scientific studies proved the development of brain identities like hindbrain, midbrain and forebrain, within the brain organoid without adding inductive signals (47). It has been shown that the maintenance of neural tissue in 3D floating culture could result in self-organizing and developing a histologically tissue architecture similar to the first trimester of brain development (47, 57). However, without the structural support of a basement membrane, the organoids' epithelium lack proper orientation, and to help this situation, hydrogels such as Matrigel composed of extracellular matrix proteins have been used (57). Overall, the generation of cerebral organoids from hiPSCs is a multi-step process that provides a better understanding of brain function by reproducing many *in vivo* characteristics of the brain when compared to a simple monolayer of neuronal cells. Certainly, cerebral organoids allow a deeper study of human

neurological conditions that have been carried out in animals so far or *in vitro* using less heterogenous and complex methods such as the rosettes in 2D or neurospheres in 3D (64).

2. Aims and hypothesis

OGG1 has been implicated in regulating brain function by canonical and non-canonical activities but its role in the human brain remains to be establish. To investigate an impact of OGG1 on human brain development, the aim of this project is to establish hiPSCs deficient in *OGG1* using the CRISPR/Cas9 editing technology and to further generate cerebral organoids. In addition, non-edited hiPSCs and subsequent cerebral organoids at different stages will be analyzed for neuronal marker genes and protein expression as well as level of DNA base lesions and epigenetic DNA modifications. The results will be compared to hiPSCs and cerebral organoids deficient for *OGG1* after successful CRISPR/Cas9 editing, to evaluate the contribution of OGG1 to neuronal development and establishment of epigenetic features.

We hypothesize that OGG1-dependent oxidative DNA damage repair is important for epigenetic remodelling and transcriptional regulation in the human brain and that loss of OGG1 will subsequently impair proper neuronal development of cerebral organoids.

3. Methods

3.1. Cell Culture

HiPSC clones used in this study including clones 1 and 6 were generated from AG05836B which is commercially available in the Cell Culture Collection of the Coriell Institute (Camden, USA). The experimental procedures were conducted in accordance with the Health Research Act (2008, no. 44).

Cells were maintained at 37 °C and 5% CO_2 on Geltrex coated (see section 3.1.1) standard 6-well culture plates (SARSTEDT). Essential 8 (E8) (Gibco) was the medium used to provide nutrients and growth factors. On a daily basis, old medium was removed and 2 ml of fresh E8 was added onto the wells, avoiding high concentrations of toxic chemicals and ensuring enough nutrients for the cells. Approximately every four to five days, cells reached a confluence of 70-80% and cell passage was conducted. For the passage, cells were treated for 2-3 minutes with EDTA (see section 3.1.2) and split in a 1:3 ratio.

Since extensive expansion is associated with genetic and epigenetic alterations (65), cells with less than 80 as passage number were used for the experiments described in this report.

3.1.1. Coating of Culture Plates

Geltrex (Thermo Fisher Scientific) was diluted 1:100 using DMEM/F12 medium (Thermo Fisher Scientific). Each well from the 6-well culture plate was coated with 1 ml of the dilution, 0.5 ml was used to coat wells from 24-well plate (SARSTEDT), and 50 µl was for the 96-well plate (SARSTEDT). Coated plates were then incubated at 37 °C for 1-2 hours and stored at 4 °C maximum a week.

3.1.2. Passage of HiPSCs

Each well was washed with 2 ml of D-PBS (without calcium and magnesium) (Gibco) and incubated for 2-3 minutes at room temperature with 1 ml of 0.5 mM EDTA (Thermo Fisher Scientific). Both EDTA and Geltrex from the new plate were removed from the wells. Because a single well will lead to the generation of three new ones, a total of 6 ml of E8 medium was added with force into each well and 2 ml of the suspension was then transferred into a new well. The next day, cells were washed with D-PBS once before adding 2 ml of fresh E8 medium.

3.1.3. Thawing of HiPSCs

Long-term storage of hiPSCs was possible in liquid nitrogen. However, according to the Coriell Institute, the viability after recovery from cryopreservation is very low, between 0.1 % to 1 %. Cryotubes (Thermo Fisher Scientific) containing clones 1 and 6 were thawed at 37 °C in water bath and their content was transferred into 15 ml falcon tube. In order to minimize osmotic pressure, 5 ml of E8 medium with 10 μM final concentration of Y-27632 ROCK inhibitor (iROCK) (Stemcell Technologies) was added drop by drop into the 15 ml falcon. After 5 min centrifugation at 200 x g the supernatant was aspirated, and the cell pellet resuspended in 3 ml of E8 medium also supplemented with 10 μM of Y-27632. The cell suspension was finally transferred into 2 wells of a previously coated 6-well plate. The next day cells were washed with D-PBS and fed with 2 ml E8.

3.2. Generation of *OGG1*$^{-/-}$ Human Induced Pluripotent Stem Cells

The inefficiency of genome engineering in hiPSCs is still a major hurdle in current research. To overcome massive cell death after manipulation, a variety of strategies were applied and are

described below. However, to get a fully understanding of the different approaches refer to Supplementary Figure S1.

3.2.1. Preparation of the gRNA Plasmid

Three gRNA plasmids for *OGG1* were subjected to examination: construct N2 (5′-GTACGATGCCCCATGCGCCT-3′), N1 (5′- GCGCCTGGGCAGAAGCGCGC-3′), and N3 (5′-GAGTACGATGCCCCATGCGCC-3′). The online tool *Guide Design Resources* from Zhan Lab was used to design the three sets of gRNA oligonucleotides and to predict off-targets. The oligonucleotides were cloned into pSpCas9-2A-GFP (PX458) plasmid (Addgene), containing GFP to visually verify transfection, U6 promoter to drive the expression of gRNA, the nuclease Cas9, among others (Supplementary Figure S2). Constructs N1-N3 needed a 5′G base for efficient transcription by the RNA polymerase III form the U6 promoter (66).

3.2.2. Electroporation of Guide RNA

The protocol described below was modified from Lin et al. (67). The electroporation was carried out using Human Stem Cell Nucleofector Kit 1 (Lonza) according to the manufacturer's instructions. The hiPSCs with 90 % confluence were treated with 1 ml of Accutase (Thermo Fisher Scientific) and 10 µM of Y-27632 for 8 min at 37°C to obtain a single cell suspension. The 0.75x TrypLE-Select (Gibco) (1X TrypLE-S and 0.5 mM EDTA/DBPS at ratio 3:1) was also used as a dissociation reagent. Cells were incubated for 8 min at 37°C with 1 ml of TrypLE-S. A total of 5 million cells were then centrifuged at 160 x g for 5 min and resuspended with 100 µl of Nucleofactor® Solution. The cell suspension was combined with 5 µg h*OGG1* gRNAs construct in an Eppendorf tube. The solution was transferred into a cuvette, carefully to prevent formation of air bubbles at the bottom. After electroporation with the A-023 Nucleofactor® Program using

the Nucleofactor® Starter Kit (Amaxa), the samples were quickly transferred onto a coated 6-well culture plate with 2 ml of E8 medium and 10 µM of Y-27632, and placed back in the incubator at 37 °C. The next day, 2 ml of E8 with 10 µM of iROCK was added to each well. Two days after electroporation, cells were sorted for GFP (see section 3.2.1).

The dissociation of hiPSCs into single cells caused massive cell death. We then wanted to evaluate whether transient overexpression of BCL-XL, an antiapoptotic protein, would improve cell survival and the efficiency of genome editing (68). In that case, the 100 µl of cell suspension was combined with 7.5 µg h*OGG1* gRNAs construct and 2.5 µg of BCL-XL plasmid in an Eppendorf tube for electroporation with A-023 Nucleofactor® Program. Another strategy was to include 0.5 µM of Navitoclax (MedChemExpress) (also known as ABT-263), a potent BCL-XL inhibitor, 8 h after electroporation (68). In that way, the first sorting for GFP^+ cells was avoided since Navitoclax preferentially deplete cells transfected with low copies of plasmids. The old medium containing the inhibitor was removed 24 h after electroporation and 2 ml of fresh E8 medium supplemented with 10 µM of iRock was added to each well. Medium was changed daily until day 7, when cells were sorted as a single cell in a 96-well plate (see section 3.2.5).

3.2.3. Lipid-Based Transfection

To further increase transfection efficiency, Lipofectamine Stem Transfection Reagent (Thermo Fisher Scientific) was used as a substitute for the electroporation. Cells were washed and treated with 0.75X TrypLE-S for 5-6 min. Cells were then flushed with 1 ml of E8 medium supplemented with 1X Ravitacell (Thermo Fisher Scientific) until clumps of 3-5 cells appeared. Since a confluence of 30-60 % is needed the day of transfection, 250,000 cells/ well were seeded in a pre-coated 6-well plate and incubated overnight at 37°C with 5 % CO_2.

The day after, medium was changed using 2 ml of fresh E8 medium supplement with the traditional Y-27632 iROCK. Two Eppendorf tubes were then prepared as detailed in Table 1:

Table1. Lipofection components and amount per well on 6-well plate

Tube 1	Opti-MEM I medium	125 µL
	Lipofectamine Stem	5 µL
Tube 2	Opti-MEM I medium	125 µL
	DNA (834 ng BCL-XL + 1666 ng CRISPR)	2500 ng

Thereafter, tube 2 was added into tube 1 and the mix was incubated at room temperature for 10 minutes. From the mix, 250 µl were added on each well and the plate was then incubated for 8 h at 37°C with 5 % CO_2. As in the electroporation, we also included 0.5 µM of Navitoclax per well to select the transformants. The day after, wells were washed once with D-PBS and the old medium was replaced with 2 ml fresh E8 medium and 10 µM of Y-27632. GFP positive cells were checked using a fluorescence microscope also 24 h post electroporation. Medium was changed every day until day 7, when cells were sorted as single cells in 96-well plate (section 3.2.5).

3.2.4. GFP^+ Cell Sorting

Two days after electroporation fluorescence-activated cell sorting (FACS) was performed to select GFP-expressing hiPSCs. Only cells that were not treated with Navitoclax, but electroporated either with CRISPR plasmid or co-electroporated also with BCL-XL, were subjected to this sorting.
Cells were incubated at 37°C for 1 h with 2 ml of E8 medium and 1X RevitaCell (supplement containing a proprietary ROCK inhibitor). Afterwards, hiPSCs were washed once with 2 ml of D-PBS and incubated for 8-10 min at 37°C with 1 ml of 0.75X TrypLE-Select. Cells were then

collected into 15 ml falcon tube and wells were rinsed with 1 ml of E8 medium supplemented with RevitaCell. Cells were centrifuged at 160 x g for 5 min and the supernatant was removed and the cell pellet resuspend in 400 µl of E8 medium with 1X RevitaCell. Cells were sorter for GFP^+ using the BD FACSAria™ III sorter. Positive cells were seeded in one well of a 96-well plate with 100 µl of E8 medium and 10 µM of Y-27632. The 96-well plate was previously coated with Geltrex. One day after, 50 µl of E8 medium was added. On day two, half of the medium was changed and on day 4 and 6 full medium change with E8 was carried out.

3.2.5. Single Cell Sorting

Seven days after transfection, cells were sorted as single cells. Plates were incubated at 37°C for 1h with 50 µl of E8 medium supplemented with 1X RevitaCell. Wells were washed once with 50 µl of D-PBS and incubated with 1 ml of 0.75X TrypLE-Select for 8 min at 37°C. Cells were then collected into 15 ml falcon tube and wells were rinsed with 50 µl of E8 medium supplemented with RevitaCell. After 5 min centrifugation at 120 x g, the supernatant was removed, and cell pellet resuspended in 200 µl of E8 medium with 1X RevitaCell supplement. BD FACSAria™ III sorter was used to seed hiPSCs as single cells in a pre-coated 96-well plate filled with 100 µl of E8 medium and 1X RevitaCell supplement. After the sorting, plates were centrifuged at 100 x g for 5 min. On the following day, 50 µl of E8 medium was added onto each well. On day 2, half medium change with E8 was performed. From day 4 to day 14, the medium was changed every 3-4 days, and afterwards, in a daily basis until day 21.

3.2.6. Plate Duplication and DNA Sequencing

After single cell sorting, surviving hiPSC clones needed about 14 to 21 days to grow and fully cover the entire well. Plates were duplicated for both genomic DNA analysis and clone expansion

after confirmation of successful genome edition. For plate duplication, 50 µl of 0.5 mM EDTA was added for 2-3 minutes. To detach cells, 100 µl of E8 medium was added to each well with force and cells were seeded into a pre-coated 24-well plate (1well:1well). Since the number of surviving clones after sorting for single cells was extremely low, cells were maintained in cell culture until sequencing results were known. However, it is also possible to keep hiPSCs at -80°C in 10 % DMSO.

The remaining cells attached to the 96-well plate were used for DNA sequencing. After 5 minutes incubation at 37°C with 50 µl of Accutase, cells were collected in PCR tubes and centrifugated full speed for 5 min. Afterwards, 50 µl of PBS was added per tube and centrifuged again to remove any remaining Accutase. The pellet was then resuspended with 20 µl of lysis buffer (10mM Tris, 1mM EDTA, pH 8.5, 0.5% IGPAL 630 (NP-40), 0.5% Tween20, Proteinase K (10 µg/ml) and tubes were placed in the thermoblock at 55°C for 2-3h. After 20 minutes centrifugation at full speed, the supernatant was collected and heated at 95°C for 10 min to inactivate Proteinase K (Sigma Aldrich). Figure 3 illustrates the strategy for *OGG1* amplification prior to DNA sequencing. We used 5′-CACGACGACATGGTTCcAG GACGAGGCCTGGTTCTGGGT-3′ as forward primer and 5′-CACCAGCAGGACGActaGC CCACAGGGCAGGAGTGGAGG-3′ as reverse primer. These primers not only amplified *OGG1,* but also allowed the addition of barcodes through adapters. Barcodes were designed to identify and associate sequences with each of the clones. First, 20 µl final volume PCR containing 1 µl of DNA, 0.5 µl of primer forward (0.3 µM), 0.5 µl of primer reverse (0.3 µM), 10 µl of Taq Master Mix (Thermo Fisher Scientific) and 8 µl of Nuclease-free Water (Thermo Fisher Scientific) was carried out. A total of 35 cycles each of 95 °C for 15 sec and 72 °C for 30 sec, were performed in a thermocycle after a pre-treatment for 3 min at 95 °C, and 72 °C for 2 min before finishing at 4°C. The PCR products were run in a 2 %

agarose gel and then diluted 1:100 before setting the second PCR to include the barcodes. As mentioned above, these new primers had a complementary region with each of the adapters used before. The forward primer was the same for all samples, but the reverse primer differed from one sample to another (Figure 3). The PCR was also carried out in 20 µl final volume containing 1 µl of DNA, 0.5 µl of primer forward (0.3 µM), 0.5 µl of primer reverse (0.3 µM), 10 µl of Taq Master Mix (Thermo Fisher Scientific) and 8 µl of Nuclease-free Water. A total of 30 cycles each of 95 °C for 15 sec and 70 °C for 30 sec, were performed in a thermocycle after a pre-treatment for 3 min at 95 °C, and 72 °C for 2 min before finishing at 4°C. Successful amplification was checked with 2 % agarose gel. Samples were sent to Luxemburg and sequenced in Eurofins Scientific.

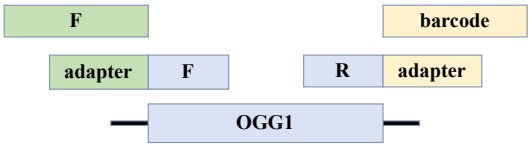

Figure 3. Sequencing strategy to identify positive hiPSC clones. Two subsequent PCRs were applied before clones were sent to Eurofins Scientific for sequencing. The first PCR allowed the amplification of the *OGG1* gene and to attach adapters on each side of the synthesized DNA. The second PCR enabled the addition of the universal forward primer, and the specific barcode.

3.3. Generation of Cerebral Organoids

The procedure to obtain cerebral organoids was conducted according to the original Lancaster, et al. protocol (57), with minor changes. The process of growing the cerebral organoids was divided into four steps.

Formation of Embryoid Bodies. HiPSCs were collected from 6-well culture plate with 70-80% confluence. The morphology of the colonies was checked under a light microscope; signatures of

differentiation could lead to aberrant EBs. A 96-well plate was used to generate EBs. Generally, a full 96-well plate with one EB per well is achieved using one well from the 6-well plate.

On day 0, cells were washed by removing E8 medium and adding 2 ml of D-PBS. HiPSCs were then incubated at 37 °C with 1 ml of Accutase for 8-10 min, time when floating colonies appeared. Cells were transferred into 15 ml conical tube containing 5 ml of DMEM/F12 and centrifuged for 5 min at 160 x g. Afterwards, the supernatant was discarded and 9000 cells were seeded on each well of a low attachment 96-well U-bottom plate (Corning) using 150 µl of Medium for EBs (Supplementary Information, Culture Media for Cerebral Organoids Development). Since it was not possible to achieve optimal EBs with the reagents listed on the original protocol from Lancaster (57), different reagents suggested in other studies were used instead (Supplementary Information, Perriot medium) (69). On day 3, the medium was changed by taking out 100 µl and adding 120 µl of a fresh medium for EBs.

Formation of a primitive neuroepithelia. On day 6, EBs were transferred into a low attachment flat-bottom 24-well plate (Corning) with Neural Induction Medium (Supplementary Information, Culture Media for Cerebral Organoids Development), seeding 1-2 EBs per well. Optimal EBs showed brightening surface with smooth edges and 500-600 µm in diameter. It was frequently seen dead cells around EBs, however, this did not comprise their correct development.

By utilizing a cut 200 µl pipette tips, the EBs were transferred from the 96-well plated into the 24-well plate filled with 500 µl of Neural Induction Medium. Pipette tips were cut with sterile scissors to obtain an opening of 1-1.5 mm in diameter to avoid disruption of the EBs.

EBs were fed with Neural Induction Medium every other day, and by day 11, EBs showed brighter and smoother edges with visible neuroepithelia around the outside.

Embedding embryoid bodies to Matrigel droplets. After thawing Matrigel (Corning) on ice for 1-2 hours, EBs were then relocated one by one onto Parafilm (Thermo Fisher Scientific) placed in a 100 x 15 mm Petri dish. First, grids of indentations were made on the Parafilm to shape the Matrigel droplets. By stretching a piece of Parafilm over an empty pipette tip tray and pressing each hole, it was possible to create small dimples on it. A grid of 6 x 6 dimples was then placed into the 10 x 15 mm Petri dish and each EB was individually transferred from the low-attachment 24-well plate into the Parafilm dimple using a cut 200 µl pipette tip. The excess of medium was removed from the dimples and 35 µl droplet of Matrigel was added into each aggregate. EBs were positioned in the center of the droplets using a pipette tip, before placing the dish in the 37°C incubator for 30 min. A total of 10 ml of Neural Differentiation Medium without vitamin A (Supplementary Information, Culture Media for Cerebral Organoids Development) was then sprayed into the Parafilm sheet until the Matrigel droplets fell on a new 100 x 15 mm Petri dish. Forty-eight hours later, the medium was changed.

After 4-5 days, when tissues began to show more complex neuroepithelia with some budding outgrowth, a cut 2 ml pipette was used to transferred 15-20 organoids to 90 x 15 mm Petri dish containing 5 ml of Neural Differentiation Medium with vitamin A (Supplementary Information, Culture Media for Cerebral Organoids Development). The dish was placed in a magnetic stirrer set at 70 rpm. Organoids were maintained for 1 month and the medium was changed every 4 days. As Figure 4 illustrates, samples from hiPSCs, 6 days EBs, and 1-month-old organoids were taken for quantification of gene expression, epigenetic modifications and 8-oxoG lesions.

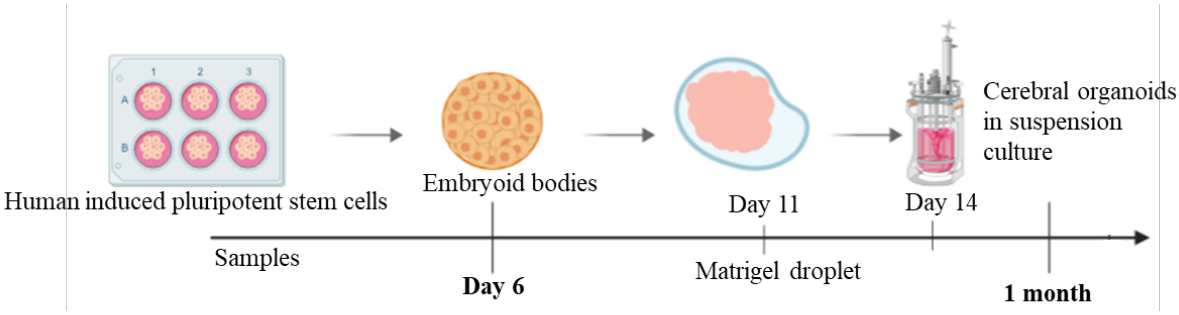

Figure 4. Overview of cerebral organoid development. Gene expression was analyzed in key stages of the organoid development: hiPSCs, EBs and 1-month organoids. EBs were fully formed from hiPSCs on day 6 and embedded in Matrigel on day 11. Around day 14, neuroepithelial bud outgrowth was visualized and cerebral organoids were placed in a magnetic stirrer from day 15 to day 31.

Other approaches: In 2018 Qian X et al. (70) published a protocol for the generation of brain region-specific organoids. Compared to Lancaster's protocol, this new method was easier: less time-consuming, less human handling and easier steps. Therefore, we developed and tested a new protocol taking the procedures from Qian's article, and the reagents listed in Lancaster's protocol since the aim of this project was to generate self-organizing cerebral organoids and not brain region-specific organoids.

3.4. Gelatin Embedding of 1-Month-Old Organoids

One organoid was placed in each of the wells of a standard 24-well plate using a cut 1-ml pipette tip. The medium was removed, and the organoids were washed once with 1 ml PBS. A total of 500 µl of 4 % paraformaldehyde (PFA) was added on each well and incubated at 4 °C for 15 min. PFA was then aspirated and the organoids were washed with PBS three times for 10 min. Organoids were kept overnight at 4 °C with 1 ml of 30 % sucrose solution.

The following day, 7.5 % gelatin/10 % sucrose embedding solution was warmed at 37 °C for 20-30 min before pouring a small amount in a medium-sized weighing dish, enough to cover the

bottom of the dish. To allow polymerization, dishes were kept at 4 °C while the 30 % sucrose solution on the organoids was being replaced with 1 ml of warmed gelatin/sucrose solution. Organoids were placed in the incubator at 37 °C for 15 minutes. Using a cut 1-ml pipette tip, the organoids were transferred from the 24-well plate to the gelatin/sucrose to the weighing dish. After 2-3 min, once the gelatin/sucrose from the organoids solidified, warm gelatin/sucrose solution was poured on the weighing dish to completely cover the tissues. Blocks were placed at 4 °C for 15-20 min, then at -20°C for 30 min, and finally stored at -80 °C. Sectioning on microtome-cryostat using the optimal cutting temperature compound (OCT) (Thermo Fisher Scientific) has been proven to be easier. Therefore, samples were embedded in OCT after cutting with scalpel the remaining gelatin, leaving only small piece of gelatin around the organoids.

Sections were cut 20-µm in the Cellular & Molecular Imaging Core Facility at the Faculty of Medicine and Health Sciences, NTNU. Afterwards, the slides were kept in the freezer.

3.5. Immunofluorescence

The slides were dried at room temperature and hydrophobic circles were drawn around the tissues with Dakpo Pen. To completely remove the gelatin from the sections, PBS-T (wash buffer 0.1 %) was used for 10 min. Sections were blocked for 1 h at room temperature with 100 µl of PBS solution with 5 % normal goat serum and 5 % bovine serum albumin (BSA). Afterwards, the slides were incubated overnight at 4°C with 100 µl of the primary antibody (Supplementary Table 1) diluted in PBS with 0.5 % normal goat serum and 0.5 % BSA. The next day, the slides were incubated for 1 hour at room temperature with the secondary antibodies Alexa 594 (goat anti-rabbit) (Thermo Fisher Scientific) and Alexa 488 (goat anti-mouse) (Thermo Fisher Scientific). (Supplementary Table 1), together with DAPI (diluted 1:1000 in PBS). Sections were washed 4

times with PPS-T for 10 min and once with PBS for another 10 min. After a quick rinse with ultra-pure water, slides were air dried for 5 min and mounted with VectaShield (Vector Laboratoies). Images were visualized using the Zeiss confocal microscope (Core Facility at the Faculty of Medicine and Health Sciences, NTNU).

3.6. Purification of Nucleic Acids

RNA isolation and purification from hiPSCs, EBs and organoids were performed using the RNeasy® Mini Kit (QIAGEN) according to the manufacturer's instructions. For DNA isolation and purification, DNeasy® Blood & Tissue Kit (QIAGEN) was used following the instructions given by the company. Purity analysis and quantification were carried out using NanoDrop ND-1000 (Thermo Fisher Scientific).

Nucleic acids were isolated from 6 different hiPSCs (3 batches from AGC1 and 3 from AGC6), 6 different EBs (3-AGC1 and 3-AGC6), and 4 different organoids (3-AGC1 and 1-AGC6).

3.7. cDNA Synthesis by Reverse Transcription

The RT-qPCR was performed in a two-step assay. An initial amount of 1000 ng of RNA was converted into cDNA utilizing the High-Capacity cDNA Reverse Transcription Kit (Thermo Fisher Scientific). In the first step of this assay, a first cycle of 25 °C for 10 min, followed by 37 °C for 120 min and 85 °C for 5 min was performed in a thermocycler. Afterwards, samples were hold at 4 °C.

3.8. qPCR

The expression of *PAX6*, *NANOG, POU5F1* (OCT-4), *MAP2, DCX, TUJ1*, *NESTIN*, and the DNA glycosylases *OGG1* and *MUTYH* was analyzed in this study. The housekeeping gene *β-ACTIN* was used to normalize gene expression. The primer sequences for each gene are presented in Supplementary Table 2.

The qPCR was carried out in 10 µl final volume containing 3 µl of cDNA (1 ng/µl), 0.5 µl of primer forward, 0.5 µl of primer reverse, 5 µl of 2x SYBR Green MasterMix (Thermo Fisher Scientific) and 1 µl of Nuclease-free Water. A total of 40 cycles each of 95 °C for 15 sec and 60 °C for 1 min, were performed in a thermocycle after a pre-treatment of 50 °C for 2 min, followed by 95 °C for 10 min.

The expression of each gene was normalized to *β-ACTIN* and analyzed using the ΔΔCT method.

3.9. Liquid Chromatography -Mass Spectrometry

The epigenetic modifications 5hmC and 5mC as well as the DNA lesion 8-oxoG were analyzed from purified genomic DNA by liquid chromatography-mass spectrometry (LC-MS). First, to further improve the purity of the isolated DNA, a pre-treatment with RNase was performed. A total of 25 µl mix of 100 mg/ml RNase A (Thermo Fisher Scientific), 10 mM Deferoxamine (DFO) (Sigma Aldrich), and 10 mM Butylated Hydroxy Toluene (BHT) (Thermo Fisher scientific), was added per 100 µl of DNA. After 30 min incubation at 37 °C, the reaction was stopped on ice. Afterwards, to the microcon-30kDa (Merck), 200 µl of 0.1 M NaOH was added before 15 min centrifugation at 14000 x g. Another round of centrifugation was conducted after adding 200 µl of Optima water (Thermo Fisher Scientific). After discarding the flow-through, two more rounds of centrifugations at 14000 x g for 30 min were performed before eluting in 50 µl water with 0.1 mM

BHT and 0.1 mM DFO. The content was transferred into fresh collection tubes and a spin 1000 x g for 3 min at 4 °C, before the DNA concentration was measured using Qubit® 3.0 Fluorometer. For the hydrolysis, an amount of 2 µg of DNA per sample was used. A total of 20 µl hydrolysis master mix (Supplementary Table 3) was added on each sample. The hydrolysis efficiency control was performed using 20 µl hydrolysis master mix with 1 µg salmon sperm DNA. After 1 h incubation at 40 °C, reactions were stopped on ice and 150 µl ice-cold acetonitrile (Sigma Aldrich) was added on each sample. Samples were then lyophilized at -80 °C and redissolved in 30 µl ice-cold water. 8oxo(dG), 5hm(dC) and 5m(dC) were analyzed by LCMS using an Agilent 6495 triple quadrupole LC-MS system with an Agilent EclipsePlusC18 RRHD column (2.1 x 150 mm, 1.8 µm particle size) at 25 °C. The mass transition used was 284.1 → 168.0 m/z, for 8oxoG; 243.1 → 126.1 m/z, for 5m(dC); and 258.1 → 142.1 m/z for 5hm(dC). The mobile phases were (A) UHPLC-grade water and (B) UHPLC-grade methanol, both containing 0.1 % UHPLC-grade formic acid. The HPLC method used a flow rate of 230 µl/min with 5 % B to 0.5 min, ramp to 20 % B at 2.5 min, ramp to 95 % B at 6 min, hold at 95 % B from 6 to 7 min, ramp to 5 % at 7.2 min, and equilibration with 5 % B from 7.2 to 10.5 min. For unmodified nucleosides (dACGT), we diluted 1:10000 with Optima and analyzed them on an API5000 triple quadrupole mass spectrometer (Applied Biosystems) with an Acentis® Express C18 column (0.5 x 150 mm, 2.7 µm particle size) at 40 °C. The HPLC method used a flow rate of 200 µl/min with an isocratic flow of 22 % B for 3 min. The mass transitions used were 252.1 → 136.1 m/z, 228.1 → 111.9 m/z, 268.1 → 152 m/z, and 243.1→127 m/z for dA, dC, dG, and dT, respectively. The PhD candidate from the Department of Clinical and Molecular Medicine at NTNU, Tobias Sebastian Obermann, performed the analysis on the mass spectrometer from the Proteomics and Modomics Experimental Core Facility at the Faculty of Medicine and Health Sciences, NTNU.

3.10. Statistical analysis

The statistical analysis was conducted with the software GraphPad Prism version 8.0. All data was normalized to hiPSCs. Shapiro-Wilk test was conducted to check whether data followed a Gaussian distribution and Bartlett's test to assess the homogeneity of variances. Results are presented as mean ± standard error of the mean (SEM). Both One-way analysis of variance (ANOVA) and Two-way ANOVA, together with Dunnett's multiple comparisons post-hoc test, were used to determine significant statistical differences between hiPSCs-EBs and hiPSCs-organoids. The level of statistical significance was set at $p < 0.05$.

4. Results

4.1. Generation of *OGG1* Deficient HiPSCs

From the three gRNA constructs available for this project, construct N2 was preferentially chosen to obtain OGG1 knock out hiPSCs. Pre-tests showed better transfection efficacy with N2 compared to N1 and N3 after the first sorting for GFP^+ hiPSCs cells (Supplementary Figure S3). However, 99.99% of the cells were either not transfected or dead after the first sorting. The Nucleofactor® programs X-003, X-005 and X-007 (Amaxa), previously used in our laboratory to successfully transfect fibroblast, were compared with the efficacy of the A-023 program shown to be efficient in Lin et al. (67) (Supplementary Figure S4). Even though the transfection efficacy was better with the program X-007 compared to A-023, the cell survival rate was extremely low. Therefore, we performed the subsequent electroporation with the A-023 Nucleofactor® Program and construct N2.

Every attempt to obtain knockouts following the steps described in Lin's protocol resulted in massive cell death after electroporation and differentiation of hiPSCs following cell sorting. Therefore, other approaches to improve the method were tested.

4.1.1. TrypLE-Select Supports Cell Survival after Single Cell Dissociation Compared to Accutase

Chen et al. describes different significant improvements in single cell cloning workflow for hiPSCs (71). Thus, we compared the suggested dissociation reagent 0.75X TrypLE-S with the widely used Accutase in our experiment setup. As illustrated in Figure 5, both cell survival and transfection efficacy improved with 0.75X TrypLE-S. We found that the cell population positive for GFP (P3

group) was clearly larger when the dissociation reagent 0.75X TrypLE-S was used, hence it was utilized for the subsequent experiments.

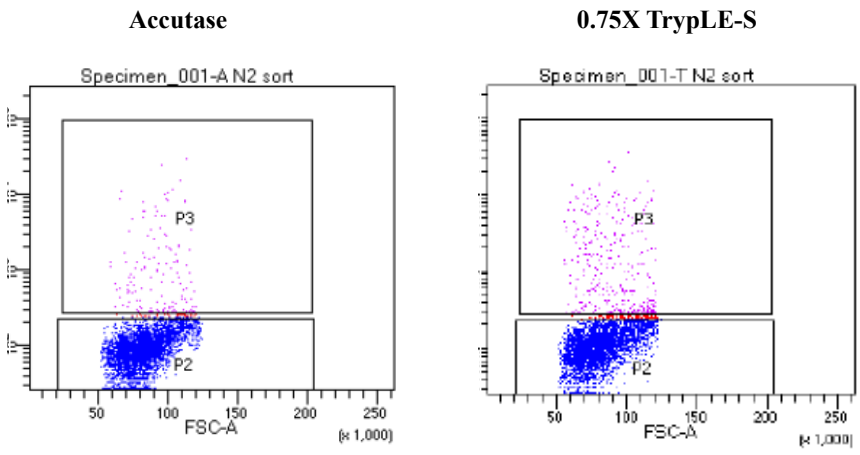

10,000	100 %	10,000	100 %	Events
3,815	38.2 %	4,139	41,9 %	Living cells
3,635	36,4 %	3,732	37.3 %	GFP negatives
137	1,4 %	360	3.6 %	GFP positives

Figure 5. Dissociation with TrypLE-S improved survival of GFP$^+$ hiPSCs. Shown are FACS plots. The y-axis indicates the GFP fluorescence whilst the x-axis represents forward scatter area (FSC-A). GFP$^+$ cell sorting revealed lower numbers of positive cells when Accutase was used as a dissociation reagent instead of TrypLE-S, 137 compared to 360.

4.1.2. RevitaCell Supports Single Cell Growth after FACS

It is widely reported that iROCKs can greatly diminish dissociation-induced apoptosis (72). The kinase domain of Rho-associated, coiled-coil containing protein kinase (ROCK), is activated after Rho-GDP binding, and the Rho/ROCK pathway is involved in mechanisms ranging from cell permeability, migration, proliferation to apoptosis. Therefore, the binding of iROCKs to the kinase domain, induce the inactive form of ROCK and prevents apoptosis (73). The traditional iROCK Y-27632 is the most common type of iROCK used for stem cells. However, Chen et al. proved

that while RevitaCell Supplement supported single cell growth after sorting by flow cytometry, the traditional Y-27632 did not have any impact on cell survival (71). Therefore, we decided to treat hiPSCs with RevitaCell before sorting by flow cytometry. According to the manufacturer, the improvement in RevitaCell is due to the more specific iROCK coupled with antioxidants and free radical scavengers.

4.1.3. Transient BCL-XL Overexpression Increased Both Single Cell Survival and Editing Efficiency after Electroporation of CRISPR/Cas9 Plasmid

The dissociation of hiPSCs into single cells caused massive cell death. Interestingly, a recent publication of Li and colleagues showed that transient overexpression of BCL-XL, an antiapoptotic protein, not only increased cell survival after electroporation but also improved the efficiency of genome editing (68). Therefore, we contacted Professor Xiao-Bing Zhang from Loma Linda University, who kindly sent us the BCL-XL plasmid, pEF1-BCL-XL-wPRE, used in the original publication. The results obtained are in agreement with the work from Li et al (68). The addition of BCL-XL plasmid not only increased the total amount of living cells, but also the total number of GFP^+ cells. One day after electroporation, it was possible to visualize more GFP^+ cells in those wells where BCL-XL was overexpressed (Figure 6A). Furthermore, FACS data revealed higher numbers of living cells and GFP^+ cells when BCL-XL plasmid was co-electroporated with CRISPR plasmid (Figure 6B-C).

Without BCL-XL, the vast majority of the electroporated cells died after the first sorting for GFP^+ cells, and the few that survived, died after the second sorting. It was only possible to visualize healthy hiPSC colonies when we co-electroporated the two plasmids (Figure 6D). However, cells

tended to massively die after electroporation, but at around day 5 cells started to recover and colonies appeared.

After testing the efficacy for BCL-XL plasmid and aiming to further reduce the high mortality rate, we then included Navitoclax as a substitute for the GFP^+ cell sorting. Navitoclax mimics the BH3 domain interaction with proapoptotic proteins, preventing BCL-XL from sequestering the proapoptotic executioners Bax and Bad (74). Therefore, Navitoclax leads to the death of cells that do not overexpress the antiapoptotic BCL-XL protein. We assumed that living cells harboring the BCL-XL plasmid would also carry the CRISPR plasmid. Moreover, the addition of BCL-XL plasmid and Navitoclax increased the likelihood of having a positive clone since larger numbers of transfected cells were growing in bigger surfaces: 9.6 cm^2 (6-well plate) instead of the 0.32 cm^2 (96-well plate) (for detailed procedure, see section 3.2.2). The ratio of positive wells after sorting for single cells was approximately 1.75 in every 96-well plate.

A

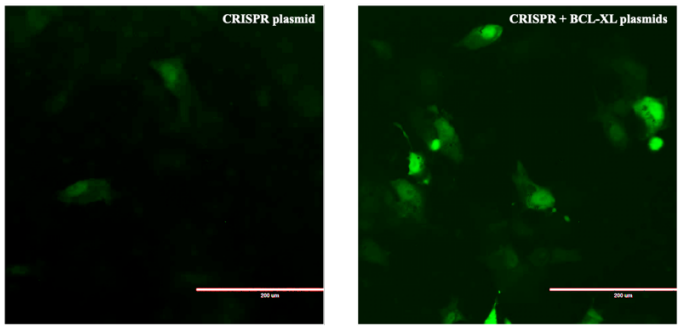

B

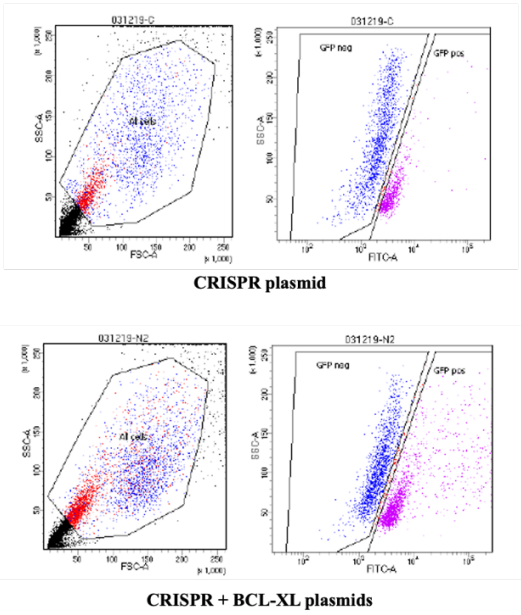

C

	CRISPR PLASMID	CRISPR PLASMID + BCL-XL PLASMID
LIVING CELLS	27.6 %	38,4 %
GFP POSITIVES	10 %	20.9 %
GFP NEGATIVES	17 %	16.6 %
NUMBER POSITIVE CELLS	2065	9005

D

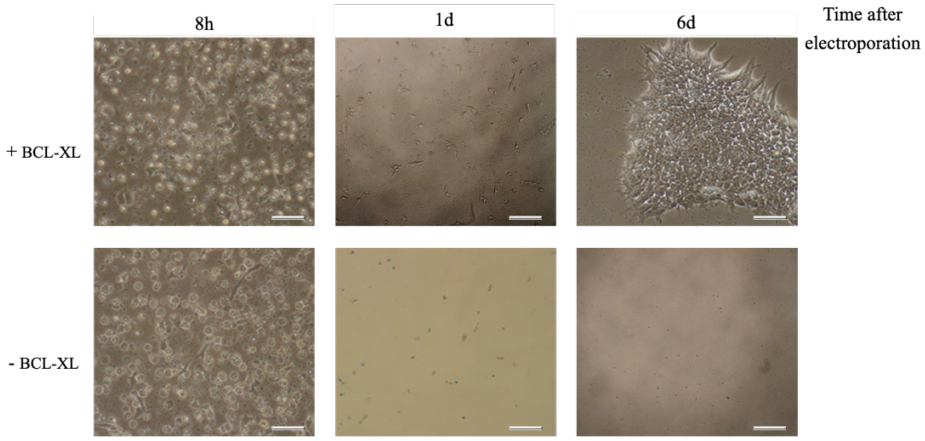

Figure 6. BCL-XL increased survival rate and editing efficiency after electroporation. (**A**) 24h after electroporation, fluorescence microscopy revealed higher number of GFP^+ cells when BCL-XL was present. Scale bars = 200 µm. (**B-C**) The number of living cells was greater when BCL-XL was co-electroporated, being the GFP^+ cells the majority. Without the plasmid, most of the cells did not carry the CRISPR plasmid (GFP^-). (**D**) 8 h after electroporation, there was no visually difference in cells transfected only with CRISPR plasmid or those carrying also the BCL-XL plasmid. However, on day 1, hiPSCs carrying the two plasmids were greater in number, and on day 6, it was only possible to see colonies in the wells were BCL-XL was included. Scale bars = 200 µm.

4.1.4. Lipofectamine Approach for Plasmid-based Genome Editing of HiPSCs

Studies describing cationic lipid delivery of plasmid DNA into hiPSCs, are very limited in number. According to the manufacturer, Lipofectamine Stem Transfection Reagent efficiently delivers Cas9/gRNA complexes while maintaining cell viability and undifferentiated state in pluripotent stem cells, therefore, we decided to test Lipofectamine in our experimental set up. In both electroporation and lipofection, cells behaved similarly the subsequent days after transfection. We observed a large number of clumps of cellular debris floating in the medium every day before the medium was changed. On day four, cells transfected with Lipofectamine Stem Cell reagent did not survive. In contrast, with the electroporation the death rate tended to decrease around day 5 and medium-sized colonies appeared.

We found that cells treated with Lipofectamine and Navitoclax, showed greater transfection efficacy than the ones treated only with Lipofectamine Stem Cell reagent (Figure 7). However, Navitoclax did not have any impact on cell survival.

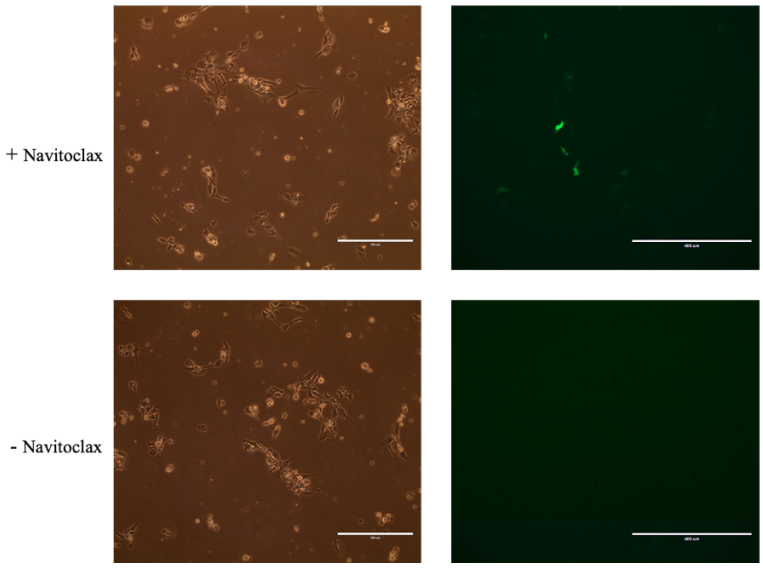

Figure 7. Navitoclax improved transfection efficiency after lipofection. 24 h after transfection, bright-field images showed similar numbers of living cells despite treatment with Navitoclax. However, Navitoclax had a great impact on transfection efficacy. It was only possible to visualize GFP^+ cells on those wells treated with Navitoclax. Scale bars represent 400 µm.

4.2. Sequencing Analysis and Knockout Confirmation

After electroporation with CRISPR and BCL-XL plasmids, and subsequent treatment with Navitoclax, 7 potentially OGG1 knock out clones derived from AGC1 (C1-C7), were obtained. As explained in the methods section, a set of adapters and barcodes were used to identify and associate sequences with each clone. Agarose gel electrophoresis allowed to verify correct amplification of the PCR products after the ligation of these adapters and barcodes. Figure 8A shows the results from the first PCR, in which the adapters were included while O*GG1* was amplified. Clear bands appeared for C3, C4, C5 and C6, however, bands for C1, C2 and C7 were not apparent. Therefore, we decided to conduct a second PCR with a 10x diluted template DNA, since the activity of DNA polymerase could be inhibited by high DNA concentration. Indeed, that was the case for C2 and C7, in which a clear band appeared in the diluted condition (Figure 8B). Figure 8C shows the PCR products from the addition of barcodes. Clear bands appeared in lanes of C2-C7, and a subtle one could be seen for C1.

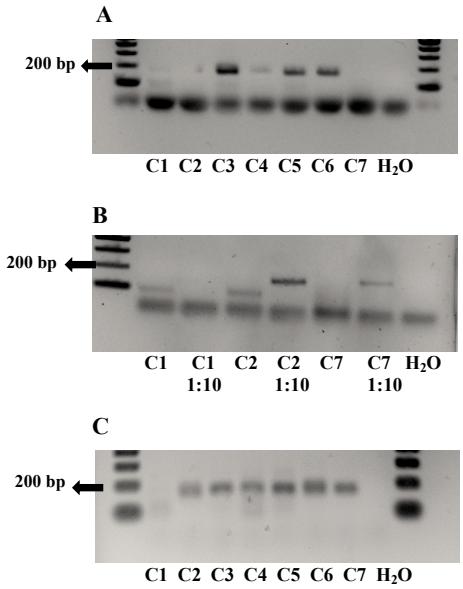

Figure 8. Agarose gel electrophoresis of *OGG1* extracted from C1-C7. (A) *OGG1* amplification and ligation of the adapters as explained in the Methods section. **(B)** A second round of Adapter PCR with 10x dilution of the template DNA for C1, C2 and C7. **(C)** PCR products after the ligation of the barcodes and universal primer.
Water was used as a negative control and the 100-bp ladder as a marker to visualize the expected 200 bp bands.

After sequencing, three clones were confirmed as *OGG1*$^{-/-}$ hiPSCs; C2, C4 and C7 showed biallelic disruption of the open reading frame after being repaired by the error-prone NHEJ.

The gRNA used was designed to target exon 1 of the *OGG1* gene, and as Figure 9 shows, all the alternative splice variants found in humans share the N-term region. Suitable frameshift mutations were found in clones 2, 4 and 7. Despite deletions and insertions observed in clone 6, the reading frame was not disrupted due to the fact that the nucleotides added or removed were a multiple of three.

The sequencing results showed that the two most common reads from clone 2 presented deletions spanning 14 and 7 nucleotides. Insertions of 1 and 2 nucleotides were found in the two alleles of clone 4. Regarding clone 7, an insertion of only 1 nucleotide was found in almost all the reads analyzed. As Figure 9 illustrates, all the mutations have occurred in the area covered by N2 gRNA.


```
ihOGG1_Nterm2      ------------------------------------------------------------  0
Ref                ------------GACGAGGCCTGGTTCTGGGTAGGCGGGGCTACTACGGGGCGGTGCCTG  48
C2_14del           ACATGGTTCCAGGACGAGGCCTGGTTCTGGGTAGGCGGGGCTACTACGGGGCGGTGCCTG  60
C2_7del            -------TCCAGGACGAGGCCTGGTTCTGGGTAGGCGGGGCTACTACGGGGCGGTGCCTG  53
C4_2ins            ----------------AGGCCTGGTTCTGGGTAGGCGGGGCTACTACGGGGCGGTGCCTG  44
C4_1ins            ---------------GAGGCCTGGTTCTGGGTAGGCGGGGCTACTACGGGGCGGTGCCTG  45
C7_1ins            ---------------GAGGCCTGGTTCTGGGTAGGCGGGGCTACTACGGGGCGGTGCCTG  45

ihOGG1_Nterm2      ---------------------------------AGGC--GCATGGGGCATCGTAC------  20
Ref                CTGTGGAAATGCCTGCCCGCGCGCTTCTGCCCAGGC--GCATGGGGCATCGTACTCTAGC  106
C2_14del           CTGTGGAAATGCCTGCCCGCGCGCTTCTGGCAT----------------CGTACTCTAGC  104
C2_7del            CTGTGGAAATGCCTGCCCGCGCGCTTCTGCCCAGGGG---------CGTCGTACTCTAGC  104
C4_2ins            CTGTGGAAATGCCTGCCCGCGCGCTTCTGCCCAGGCACGCATGGGGCATCGTACTCTAGC  104
C4_1ins            CTGTGGAAATGCCTGCCCGCGCGCTTCTGCCCAGGC-CGCATGGGGCATCGTACTCTAGC  104
C7_1ins            CTGTGGAAATGCCTGCCCGCGCGCTTCTGCCCAGGT-CGCATGGGGCATCGTACTCTAGC  104
                                                        *****

ihOGG1_Nterm2      --------------------------------  20
Ref                CTCCACTCCTGCCCTGTGG------------  125
C2_14del           CTCCACTCCTGCCCTGTGGGCTAGTCGTCCT  135
C2_7del            CTCCACTCCTGCCCTGTGGGCTAG-------  128
C4_2ins            CTCCACTCCTGCCCT----------------  119
C4_1ins            CTCCACTCCTGCCCTG---------------  120
C7_1ins            CTCCACTCCTGCCCTG---------------  120
```

Figure 9. Visual representation of genome-edited mutants. N2 gRNA targeted exon 1 of *OGG1* gene, which is common for all the alternative splice variants found in humans. The alignment was performed with the Clustal Omega program. N2 is represented as its reverse complement, ihOGG1_Nterm2. The reference sequence was included for the indels analyzes. The two most common alleles from clone 2 harbored deletions of 14 and 7 nucleotides (C2_14del; C2_7del). Insertions of 1 and 2 nucleotides were found in the two most representative alleles of clone 4 (C4_2ins; C4_1ins). Clone 7 presented an insertion of 1 nucleotide (C7_1ins).

4.3. Cerebral Organoids Derived from HiPSCs

To examine the role of the DNA glycosylase OGG1 in human brain development, cerebral organoids derived from hiPSCs were generated. As shown in Figure 10A, typical hiPSCs are round and small cells with well-defined edges that form compact colonies. Cells at the edges of undifferentiated colonies tended to lose their round morphology and begin to differentiate.

Under the light microscope, rounded shape EBs with clear and smooth borders were already seen one day after their formation. EBs increased in size up to 500-600 μm before they were transferred to the Neural Induction Medium. Figure 10B illustrates an optimal EB on day 6 showing a bright surface sign of ectodermal differentiation and a dark center with non-ectodermal tissue. It was often observed that EBs were surrounded by dead cells (Figure 10B), however, that did not affect the formation of the EB. An early organoid showing radially organized neuroectoderm is depicted in Figure 10C. Smooth edges with bright optically translucent surfaces were signs of suitable organoids. Further developed organoids started to show buds of neuroepithelia outgrowth that were optically clear (Figure 10D-E). However, small buds of translucent ectoderm lacking radial organization were also visible in many optimal organoids (Figure 10D), which did not impede the development of surrounded neuroectodermal tissue. Differences in size, complexity and cell density became greater as the cerebral organoid development progressed. Complex structures with more neuroepithelia buds and cavity formations were found in 1-month-old organoids (Figure 10F).

In the beginning, we experienced problems to generate optimal EBs following Lancaster protocol (57), therefore, different approaches were applied to find the best culture conditions. The hiPSCs clones AGC1 and AGC6 were tested for a potential lack of pluripotency, since unhealthy colonies may explain suboptimal EBs. However, EBs derived from different hiPSCs clones were also

unsuitable. Also, the efficacy of different batches of 96-well plates were compared, without any difference in the outcome of EB generation. Moreover, it was reported that both the addition of Glutamax into the medium and the use of Fetal Bovine Serum (FBS) compatible with stem cells were key to successfully generate EBs (57). Unfortunately, it was still not possible to achieve an optimal morphology, but small-sized EBs, many with big bubbles in the center and lacking clear edges. The desired rounded shape characteristic from the EBs was also not possible to achieve following the Qian X et al. procedure (70). The EBs tended to stick to each other and bubbles appeared in the middle of the EB (Supplementary Figure S5).

Eventually, optimal EBs were generated using different medium ingredients (Supplementary Information, Perriot medium) (69). Since the Knockout Serum Replacement (KSOR) (Thermo Fisher Scientific) was not included in the Perriot formulation and the other reagents from the Lancaster medium were used to generate different stages of the cerebral organoid development, we believe that KSOR was expired and causing EBs to fail.

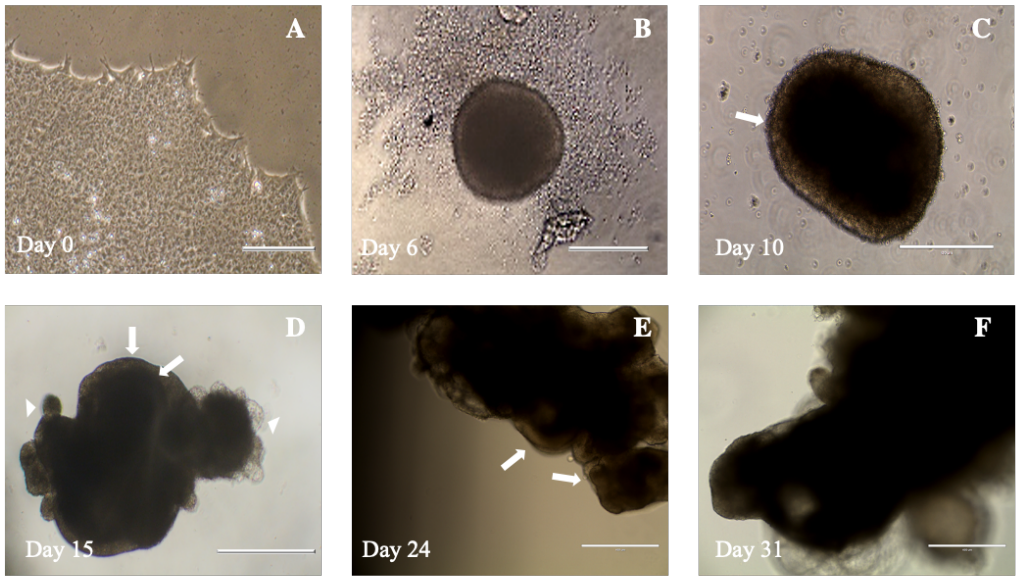

Figure 10. Stages of cerebral organoid development from hiPSCs. (**A**) Typical hiPSC colony with optimal morphology. Scale bar = 100 µm. (**B**) An EB at day 6 surrounded by dead cells and showing a bright surface with smooth edges and a dark center with non-ectodermal tissue. (**C**) An organoid on day 10 showing smooth edges and optical translucent surface consistent with neuroectoderm (white arrow). (**D**) An organoid at day 15, bigger in size with visible neuroepithelial bud outgrowth (white arrows) and outgrowths that are not neuroepithelial (arrowheads). (**E**) A more developed cerebral organoid showing multiple buds of neuroepithelial outgrowth (white arrows) with smooth and bright surfaces. (**F**) A 31-day-old organoid bigger in size and revealing more complex neural structures. Scale bars B-F, 400 µm.

In the Lancaster protocol, organoids were cultured in a spinning bioreactor, which ensured correct nutrient diffusion and enabled the generation of organoids up to 4 mm in diameter within two months (57). Instead, we chose to culture organoids in Petri dishes. Based on the experience of our laboratory, Petri dishes were not only good enough to generate organoids but also saved medium, 5 ml compared to 75 ml in the bioreactor.

4.4. Gene Expression

The relative expression of specific genes was determined for three different stages of the cerebral organoid development: hiPSC, EB and organoid. To provide a better understanding, genes are subdivided below in three different categories.

4.4.1. Pluripotency Markers

Both OCT-4 and NANOG are involved in the renewal of undifferentiated stem cells (75, 76). As Figure 11A illustrates, these stem cell markers decreased as cerebral organoid development progressed. The levels of the transcription factors OCT-4 and NANOG were highest in the pluripotent hiPSC stage and decreased significantly in EBs and organoids.

4.4.2. Neural Markers

The neuroepithelial marker NESTIN as well as PAX6 are present in radial glia (77, 78). The statistical analysis suggested a significant decrease in the expression of *NESTIN* in organoids compared to hiPSCs (Figure 11B). While the expression levels of *PAX6* greatly increased with the development of the organoids, the difference between stages was not statistically significant. This could be explained by the huge variation on PAX6 levels particularly within the organoid stage (Figure 11B).

Both DCX (doublecortin) and TUJ1 (class III β-tubulin) are markers for immature neurons (79). While there were no significant statistical differences among the groups for the expression of *TUJ1,* there was a trend towards a reduction in the expression of *TUJ1* in the organoid stage compared to hiPSCs. Regarding DCX, the expression was significantly increased between hiPSCs and EBs, however, there was no significant statistical difference between hiPSCs and organoids (Figure 11B).

Another neural marker that was evaluated in this project was MAP2, expressed in mature neurons (80). As shown in Figure 11B, there was a significant increase in the expression of this marker in EBs compared to hiPSCs. Surprisingly, a reduction in the expression of *MAP2* was found between EBs and organoids.

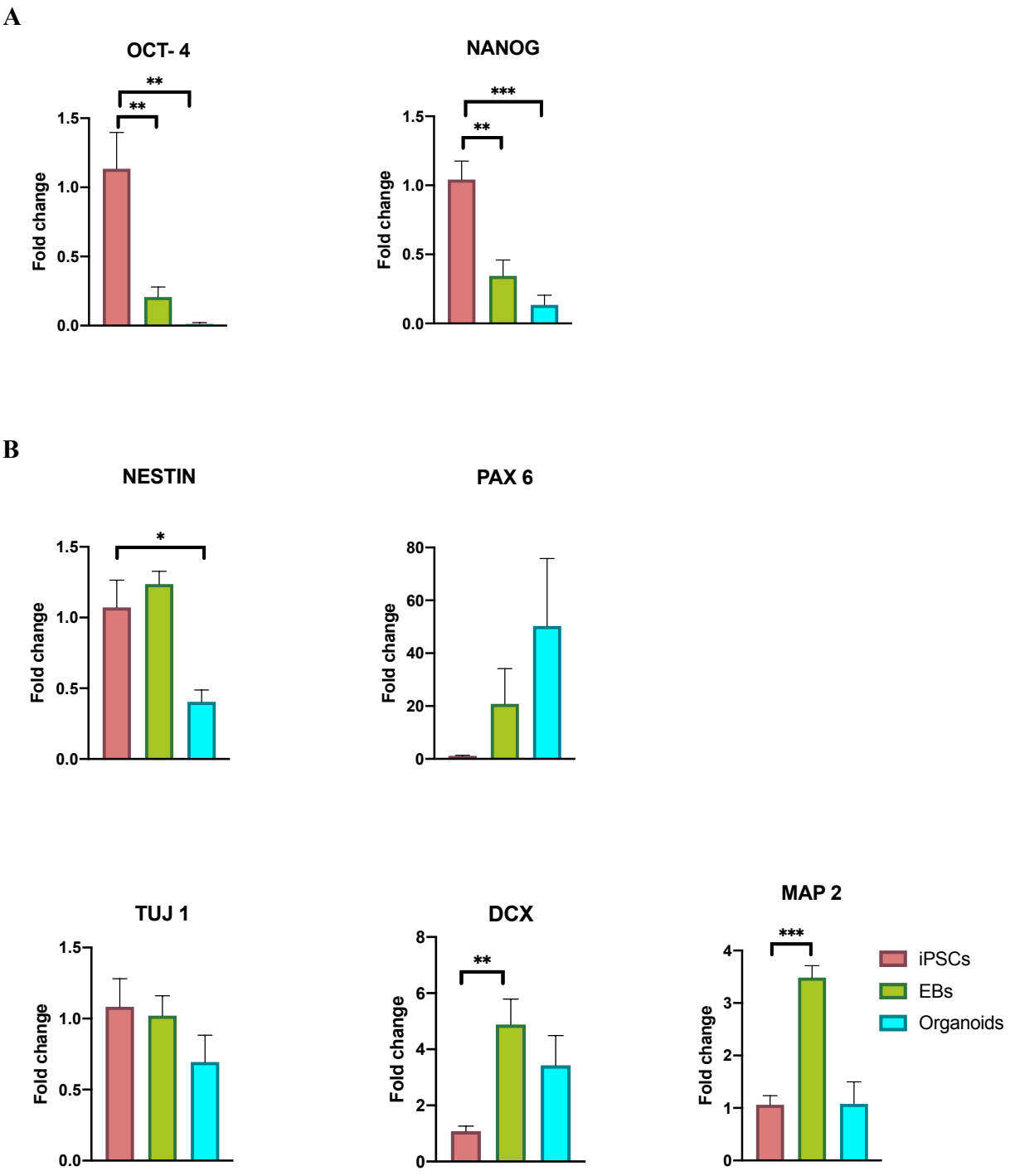

Figure 11. Difference in gene expression between hiPSCs, EBs and organoids. qPCR analysis of (**A**) pluripotency markers and (**B**) neural markers. For all cases, gene expression was normalized to the housekeeping gene *β-ACTIN* and compared to the hiPSCs stage. Y- axis indicates the log2-fold change. Error bars show the mean ± SEM. A-B, n = 4-6 samples per stage. *p<0.05; **p< 0.01; ***p< 0.001.

4.4.3. DNA Glycosylases

The relative expression of the DNA glycosylases OGG1 and MUTYH were also evaluated in the hiPSC, EB and organoid stages (Figure 12). Interestingly, the expression of *OGG1* significantly increased in EBs and organoids compared to the hiPSCs stage.

While, the expression of *MUTYH* was significantly higher in EBs compared to hiPSCs, the statistical analysis showed no significant difference between hiPSCs and the more developed organoid stage.

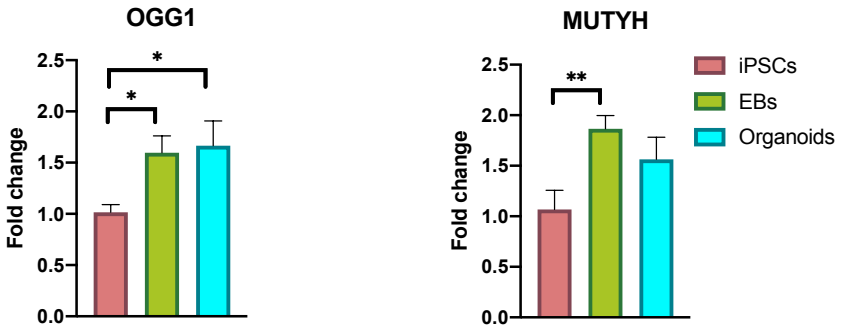

Figure 12. Expression of DNA glycosylases in hiPSCs, EBs and organoids. The expression levels of *OGG1* increased as the cerebral organoid development progressed. In consonance, *MUTYH* was also more expressed in EBs and organoids than in hiPSCs, however, EB was the stage with the highest levels. Gene expression was normalized to the housekeeping gene *ß-ACTIN* and compared to the hiPSCs stage. Y-axis indicates the log2-fold change. Error bar shows the mean ± SEM. A-B, n = 4-6 samples per stage. *$p<0.05$; **$p< 0.01$.

4.5. Protein Expression in Cerebral Organoids

Immunofluorescence staining in 1-month-old organoids revealed the formation of ventricle-like structures. (Figure 13). These formations are well described and are known as ventricle-like cavities or pseudo-cavities (57, 81). TUJ1 is found in the cell body, dendrites and axons of immature neurons (82). As shown in Figure 13A, $TUJ1^{+}$ cells (green), were found only in the ventricle-like cavities. Moreover, NESTIN is an intermediate filament protein expressed in

progenitor cells such as radial glia (83). Despite the poor-quality of the antibody, we could see $NESTIN^+$ cells (red) not only in the body of the organoid but also in the pseudo-cavities.

Nuclear staining with PAX6 (green) showed radially organized progenitor cells around the pseudo-cavities (Figure 13B).

DCX is a microtubule-associated protein, which is a marker for migrating neuronal progenitor cells (neuroblasts) and immature neurons (84). Interestingly, this marker was expressed on the edges of the ventricle-like cavities. In general, DCX^+ cells were located in the periphery of $PAX6^+$ cells, however, as Figure 13B illustrates, some cells expressed both PAX6 and DCX, indicating a transition towards a more differentiated stage.

A

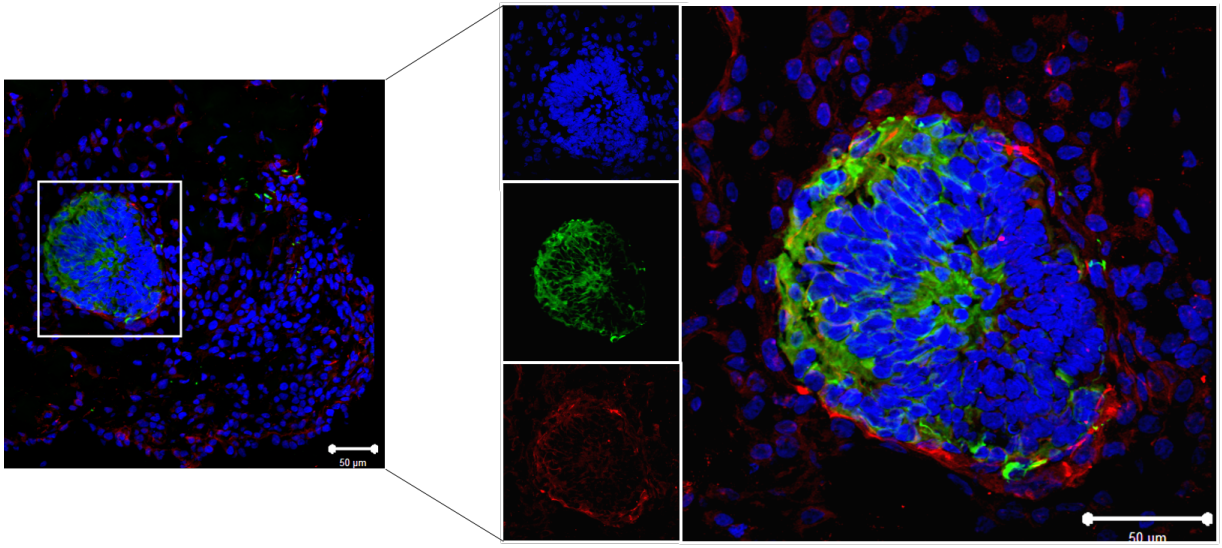

B

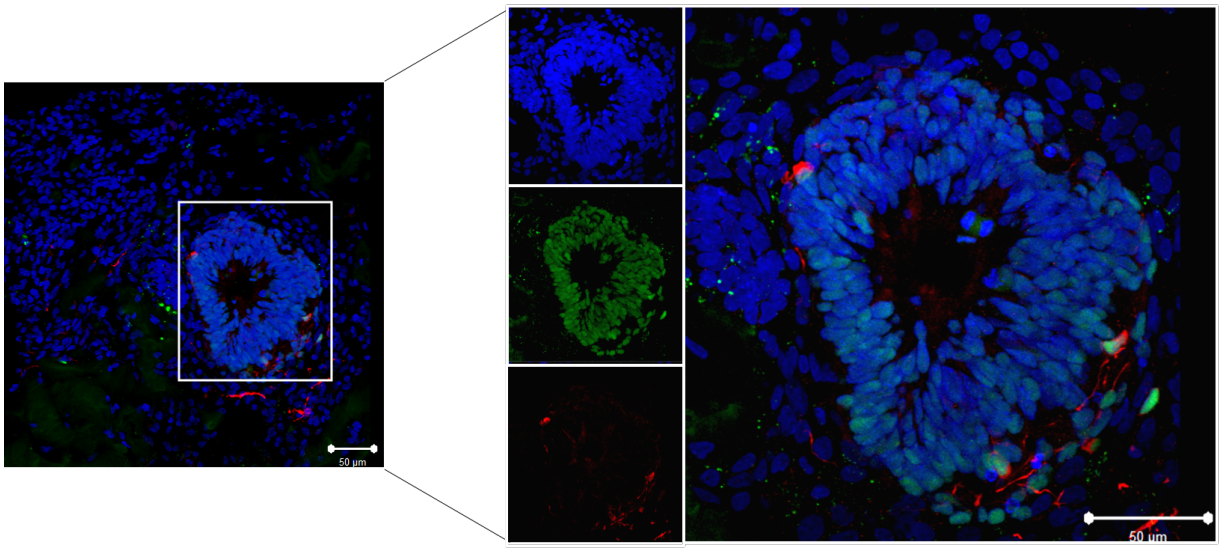

Figure 13. Immunofluorescence for radial glia and neural processes. 1-month-old organoids were stained for **(A)** TUJ1 (green) and NESTIN (red), and **(B)** PAX6 (green) and DCX (red).
DAPI (blue) was used to visualize nuclei. Images were magnified from 20x to 40x to show ventricle-like cavities. Scale bars = 50 µm.

4.6. Quantification of Epigenetic Modifications and 8-oxoG Lesion

Levels of 5hmC were found to be higher in hiPSCs compared to EBs or organoids (Figure 14A). However, One-way ANOVA with Dunnett's multiple comparisons post-hoc test showed close to significant statistical difference between hiPSCs and EBs (p=0.059), but no difference between hiPSCs and organoids (p=0.198), although the trend to reduced 5hmC level was similar.

Among the three developmental stages, the highest levels of 5mC were found in hiPSCs. However, no significant statistical difference was found among the groups (Figure 14B).

Regarding the OGG1 substrate 8-oxoG, there were no significant statistical differences in the levels between the three stages (p>0.05). As Figure 14C illustrates, the levels of 8-oxoG were similar between hiPSCs and organoids, but slightly reduced in the EB stage.

Interestingly, absolute levels of 5mC, 5hmC, 8-oxoG from AGC1 and AGC6 differed considerably, therefore, each clone was treated separately, and results are presented in Supplementary Figure S6. AGC6 clone exhibited lower levels of modifications compared to AGC1, however, the trend towards reduction during organoid development was similar. While there were no significant differences in 5mC and 8-oxoG levels in AGC1 clone, we found a significant decrease in 5hmC levels in EBs and organoids compared to hiPSCs. For AGC6 clone, the difference in the levels of modifications was not significant among the stages (Supplementary Figure S6).

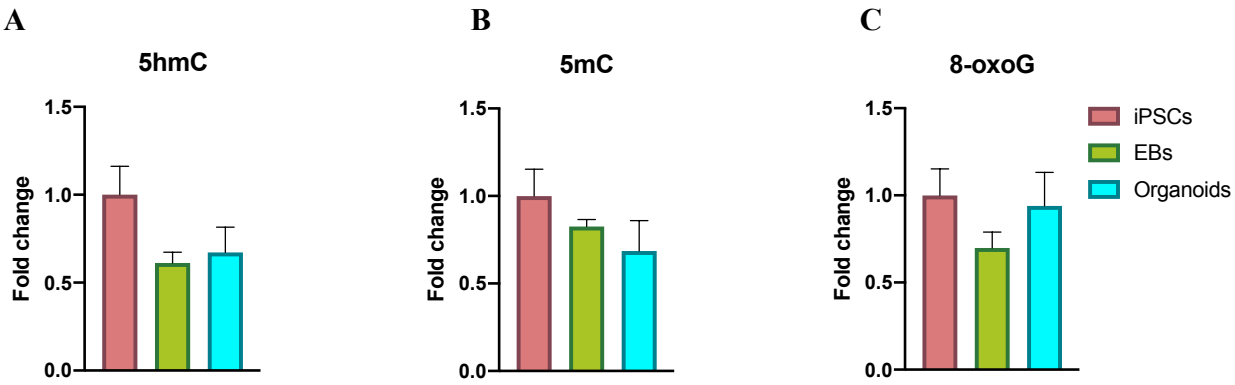

Figure 14. Relative changes of 5hmC, 5mC and 8-oxoG levels during cerebral organoid development. (**A-B**) There was no significant statistical difference in the epigenetic modifications 5hmC and 5mC levels between the groups. However, hiPSCs harbored greater levels of these modifications. (**C**) 8-oxoG levels were reduced in the EB stage, however, One-way ANOVA showed no significant statistical difference between the groups.
Error bar shows the mean ± SEM. Control = hiPSCs. A-C, n = 4-6 samples per stage.

5. Discussion

The DNA glycosylase OGG1 prevents mutations caused by 8-oxoG, which is introduced in DNA bases as a result of ROS activity. ROS production increases with age and is also higher in neurodegenerative diseases such as Parkinson, Alzheimer and amyotrophic lateral sclerosis (85). Moreover, OGG1 has been associated with critical brain functions and neurogenerative diseases (86). To the best of our knowledge, there are no studies reporting *OGG1*-deficient hiPSCs. We believe that the further development of cerebral organoids from these genetically modified cells, will give new insights and valuable information about human-specific features on oxidative stressed-related neurodegenerative diseases and will elucidate the role of OGG1 in human brain development.

5.1. Discussion on Methods

5.1.1. Genome Editing in HiPSCs

Electroporation was a better technique for plasmid delivery into hiPSCs than lipid-based transfections. However, massive cell death and cell differentiation was observed every time the electroporation was performed according to Lin et al. procedure (67). As widely stated in literature, this was explained by the sum of three factors: anoikis, apoptosis induced by the dissociation of hiPSCs into single cells; the cell death caused by electric shock during electroporation; and the cleavage of the genomic DNA (80). Moreover, sorting for GFP^+ hiPSCs and subsequent single cell sorting led also to massive cell death. Here, we and others reported that the transient overexpression of the antiapoptotic protein BCL-XL is a powerful tool for the generation of edited hiPSCs (68). Without transient BCL-XL transfection, the tremendous cell death in hiPSCs as a consequence of any type of manipulation, made it impossible to obtain a single clone deficient in

OGG1. To include Navitoclax in the protocol was an effective way to enrich transfected cells and avoid the high death rate on hiPSCs due to flow cytometry. As speculated by the authors, cells harbouring more copies of BCL-XL and CRISPR plasmids, were more prone to survive the selective pressure induced by Navitoclax (68).

Even though AGC1 and AGC6 clones were generated from the same AG05836B donor, AGC6 was more sensitive to manipulation. Therefore, it was only possible to obtain *OGG1*$^{-/-}$hiPSCs from AGC1 clone. DNA sequencing confirmed knockout hiPSCs, however, further analysis of OGG1 protein expression with Western Blot should be considered. Moreover, it is of interest to test whether the improved survival rate after BCL-XL transfection, together with the high transfection efficacy of the Nucleofactor® program X-007 (Supplementary Figure S4), would increase the number of knockout clones. Future experiments may also involve the electroporation of other CRISPR constructs such as N1 or N3 to minimize unwanted off-target effects. Some of these experiments could have been part of this project, however, the extraordinary situation arising from SARS-CoV-2 pandemic, caused to stop these experiments.

Overall, we could optimize the protocol for gene edition and successfully generate *OGG1* deficient hiPSCs. However, the low editing efficiency due to the massive cell death hampers the genetic modification of hiPSCs and the development of further tools for functional genomics, disease modelling and regenerative medicine. The undeniable potential harboured in edited hiPSCs, merit further investigations to facilitate their genetic manipulation while increasing cell survival.

5.1.2. Cerebral Organoids

Cerebral organoids are a powerful tool able to recapitulate human brain's development, function and disorders (87). Brain organoids derived from hiPSCs enables the study of processes that are uniquely regulated in humans and cannot not be addressed using animal models (88).

However, current methods to generate cerebral organoids need further improvements and optimizations. We experienced a great difference in cell density, shape and size between cerebral organoids from same batches. These results are in accordance to literature and are in fact, a huge problem that hinders the use of organoids as a reliable model for experimentation.

While cerebral organoids could be maintained for more than 1 year (57), due to the difficulties that we experienced with the generation of EBs, it was only possible to develop 1-month-old cerebral organoids. The decision to culture the organoids in Petri dishes instead of the spinning bioreactor, may have had a negative impact. The importance of working with successful bioreactors to reduce variability between organoids has been reported. In addition, organoids can generate different structures such as forebrain or retinal tissues depending on the environment of the bioreactor (89). We observed that 1-month-old organoids were still attached to Matrigel and many of them were in a suboptimal shape showing an evident lack of cell density. We believe this is partially explained by the fact that those organoids were cultured in Petri dishes instead of spinning bioreactors.

HiPSCs are considered to be one of the most difficult cell types to culture. Cells tended to die massively or differentiate after thawing from liquid nitrogen as well as during routine tasks such as cell passaging. The development of cerebral organoids derived from clone AGC6 was considerably more challenging than with AGC1.This variability was not only observed between cell clones, but also on cell passages, colonies from the same well, and even between cells within a colony. Another limitation is that despite several published methods allow the generation of brain

regional identities, none of them are able to mimic the developmental and pattering cues essentials during human brain development (47). The lack of embryonic axes that guide the directionally of brain development, hinders the organization within the brain organoids that resembles the brain *in vivo* shape or pattern (87). Improvements such as organoids with vasculature-like networks would not only provide a better supply of oxygen and nutrients, but also axial pattering. (47).

One aim of this project involved the development of cerebral organoids from hiPSCs deficient in *OGG1.* Whilst the generation of cerebral organoids from non-modified hiPSCs was possible, the time taken to generate successful knockout cells covered almost the entire Master Thesis. Despite being very ambitious with this initial aim, to actually optimize the protocol and generate *OGG1*$^{-/-}$ hiPSCs was already a milestone taking into account the low chances of success and the limited amount of time.

Overall, cerebral organoids are a powerful tool that have brought the scientific community one step closer to get a fully understanding of neurological diseases. However, many changes and optimization in the procedure still need to be made, mostly focused on generation of less variable organoids.

5.1.3. Immunofluorescence

Embedding organoids straight in OCT instead of gelatin should be considered for further experiments. Not only is it easier to cut with the microtome, but also it avoids repeated freezing thawing that can negatively impact tissue structure and quality of the staining. Moreover, once the block was frozen it was very difficult to distinguish the exact position of the organoid. To stain with erythrosine before embedding would reveal more clearly the position of the organoid since it stains organoid surfaces and does not interfere with immunofluorescence.

5.2. Discussion on Results

5.2.1. Gene Expression

During cerebral organoid development, differential gene expression was observed among the three stages analyzed. A robust expression of the pluripotency markers *OCT-4* and *NANOG* was detected in hiPSCs. In consistency with Xie and colleagues, the expression of these markers was abruptly lost in EBs and continued to decrease in organoids (90). OCT-4 and NANOG are stemness factors that control both self-renewal of undifferentiated hiPSCs and maintain their pluripotency (75, 76). Therefore, we expected to see a significant drop in their expression as stages progressed. Regarding the neural progenitor markers PAX6 and NESTIN, Ferguson and colleagues found that once the EB is formed, both markers are downregulated as differentiation processed (91). We could see these changes for *NESTIN* expression, since there was a dramatical drop from the EB to the organoid stage. However, PAX6 levels kept increasing reaching the highest expression in the organoid stage. Interestingly, Watanabe et al. reported that cells growing in a medium supplemented with B27 (without vitamin A), showed an increase in the expression levels of *PAX6* (92). EBs at day 6 were less time under the influence of B27 supplement than 1-month-old organoids. It is also important to consider that the variability amongst organoids could also affect gene expression. Indeed, PAX6 levels from AGC6-derived organoids were lower than in the EB stage, resulting in a large standard deviation in the organoids group.

The microtubule-associated protein, DCX, plays an essential role in the migration of neurons in the human brain (84). DCX together with TUJ1, are markers for immature neurons (79). Lancaster and Knoblich reported that after 1 month in culture, cerebral organoids may start exhibiting the expression of these two markers (57). Therefore, we assumed to find more expression in the organoid stage. However, we did not see significant changes in the expression levels of *TUJ1*

between the three stages analyzed. In addition, the expression of DCX was higher in the EB stage compared to 1-month-old organoid. This could be explained by three factors: (1) variability between organoids, (2) suboptimal and immature organoids, or (3) biased gene expression due to inappropriate medium formulation. As explained in section 4.3, it was not possible to generate suitable EBs with the reagents listed in the Lancaster protocol (57). By the time we suspected that KSOR was causing EBs to fail, it was more feasible to produce EBs with the combination of different substances already available in our laboratory rather than ordering new KSOR. Optimal EBs were generated with the medium formulation reported by Perriot and colleagues, which included the supplements B27 and N2, both important for neuronal differentiation and survival (69).

Some reports showed a slight increase in MAP2 levels on 35 days organoids compared to hiPSCs (93). However, the expression of *MAP2* was better defined in more mature organoids, 2.5-3 month old (94). As expected, we did not see differences in *MAP2* expression between hiPSCs and 1-month-old organoids. However, the expression of this marker on EBs was considerably higher than in the two other stages. This could also be explained by the use of B27 and N2 supplements for EBs culture that drives EB already into a neuronal stage.

These experiments should be repeated with the formulation listed in Lancaster protocol and evaluate whether these results are reproducible.

5.2.2. Immunofluorescence for Radial Glia and Neural Processes

Neurogenesis in human cerebral cortex occurs at two major proliferative zones, the ventricular zone and the subventricular zone. Neuroepithelial cells transition to radial glia which, in turn, produce neurons and intermediate populations such as intermediate progenitors and basal radial

glia. While radial glia are located in the ventricular zone, radial basal glia are located in the subventricular area (47). Both radial glia and basal radial glia express PAX6 and NESTIN (95). Similarly, in 1-month-old organoids, cells from the ventricles-like cavities also expressed both PAX6 and NESTIN. Moreover, it is reported that TUJ1, which is a marker for immature neurons, is abundant in the interface between the ventricular and subventricular zones (96). In agreement with these reports, we found that TUJ1 was only expressed in the ventricle-like cavities in the organoids. DCX was expressed in the edges of the ventricle-like cavities, which resembles the *in vivo* outward migration of more differentiated cell types.

Overall, ventricles-like cavities resemble the proliferative zone from human cerebral cortex, suggesting that brain organoids successfully mimic features of cortical development.

5.2.3. DNA Glycosylases and Brain Development

To evaluate whether the DNA glycosylases OGG1 and MUTYH could influence human brain development, their expression levels were studied on three different stages of the cerebral organoid development. To the best of our knowledge, there are no studies analysing the expression of *OGG1* and/or *MUTYH* in brain organoids.

Interestingly, the expression levels of *OGG1* increased as the cerebral organoid development progressed. The amount of *OGG1* transcribed was significantly higher in EBs and organoids compared to hiPSCs, suggesting a role of OGG1 in brain development. These preliminary results are aligned with studies carried out in zebrafish embryos, in which *Ogg1* was highly expressed in the brain during early embryonic development. Lack of *Ogg1* in zebrafish embryos caused changes in brain volume and integrity, imbalance and motor impairments (97). Similarly, *Ogg1* deficient

mice showed impaired cognition and behaviour (34). Therefore, it will be interesting to study differences in the structure of cerebral organoids develop from *OGG1*$^{-/-}$ hiPSCs.

The relative expression of DNA glycosylase MUTYH was also evaluated in hiPSCs, EBs and organoids. The highest expression was found to be in the EB stage. In contrast to OGG1, MUTYH levels did not increase in the organoid stage. To further support these results, the enzymatic activity of OGG1 and MUTYH should be analyzed. This was the first report that studied the expression of DNA glycosylases in a human brain model, we believe that by enlarging the sample size, even more interesting and significant results will be obtained.

5.2.4. Epigenetic Modifications and 8-oxoG Lesion

Since 5mC is oxidized to 5hmC by the TET family proteins, these epigenetic modifications are closely related. Therefore, it was not surprising to see similar dynamics during the cerebral organoid development. The levels of 5hmC and 5mC were lower in the EB and organoid stages compared to the hiPSC. A study using epigenome-wide sequencing, revealed that the epigenomic state of cerebral organoids resembled early-to-mid human fetal brains. Interestingly, the authors found a massive demethylation of pericentromeric repeats after neural differentiation that was not present during the fetal brain development (98). These findings could explain the observed decrease in 5mC and 5hmC levels in EB and organoids. Culture medium supplemented with B27 and N2 could have induced neural differentiation and the consequent demethylation on EBs.

The amount of 8-oxoG measured in hiPSCs and organoids were similar. The 8-oxoG lesion is repaired by OGG1 and MUTYH and we found that EBs presented lower levels of 8-oxoG, the stage when *MUTYH* and *OGG1* increased in expression. Moreover, a role of 8-oxoG beyond DNA damage has been reported. Fleming and colleagues demonstrated that when 8-oxoG was generated

in the promoter region of certain genes, it enhanced their expression through the BER pathway (99). These findings indicate that 8-oxoG could also act as a DNA epigenetic modification. Future experiments in hiPSCs should assess the impact of *OGG1* deletion on gene expression and epigenetic marks. Since 8-oxoG lesion is repaired by OGG1 and MUTYH glycosylases (Figure 1), it will be interesting to see whether the lack of OGG1 will result in a compensation mechanism with MUTYH or differences in 8-oxoG levels and neural markers during cerebral organoid development. Moreover, promoter regions of genes involved in immune response and oxidative stress such as the vascular endothelial growth factor (VEGF), are substrates for OGG1 (99) through 8-oxoG. Therefore, the analyses of these genes in *OGG1*$^{-/-}$ hiPSCs should also be considered.

6. Conclusion

This project successfully applied state-of-the-art technology including genome editing in hiPSCs using CRISPR/Cas9 and generation of cerebral organoids. Not only were *OGG1* deficient hiPSCs generated, but the protocol for gene editing was optimized and can now be easily applied for generation of gene knock outs. To include BCL-XL and Navitoclax in the protocol makes it reliable and time-efficient. While there are many improvements to be made to further increase cell survival, this thesis provides a valuable method to generate knockout hiPSCs in less than a month. We also aimed to develop cerebral organoids deficient for *OGG1* to evaluate the contribution of this DNA glycosylase to neuronal development and establishment of epigenetic features. However, the time required for these experiments exceeded the duration of this project. We found that *OGG1* expression increased as the cerebral organoid development progressed, therefore, we believe that loss of *OGG1* might impair proper neuronal development on cerebral organoids. It will be interesting in the future to investigate the development of cerebral organoids derived from the *OGG1*$^{-/-}$ hiPSCs generated in this project.

Moreover, the results obtained from gene expression in the three stages analyzed were similar to other studies, suggesting that cerebral organoids are a reliable model that truly recapitulate early stages of human brain development. However, the organoid model still needs to be optimized. The variability between organoids and their considerable cost of production, are two key drawbacks that stop their widespread use in laboratories as *in vitro* models.

7. Supplementary Information

7.1. Supplementary Figures

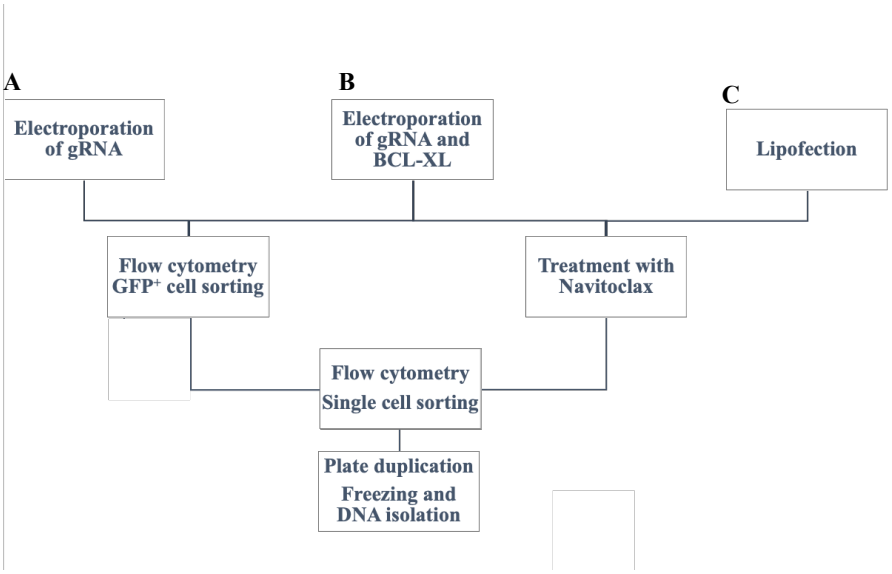

Supplementary Figure S1. Strategies to generate *OGG1*$^{-/-}$ hiPSCs. In strategy A, 2 days after the electroporation of the gRNA, cells were sorted for GFP. In strategy B, cells were co-electroporated with CRISPR plasmid and BCL-XL plasmid. As happened in strategy A, 2 days after co-electroporation, cells were also sorted for GFP. However, in parallel hiPSCs were treated with Navitoclax to evaluate whether the addition of the BCL-XL inhibitor increased survival rate. For the third strategy (C pathway), hiPSCs were transfected for 24h with Lipofectamine Stem Transfection Reagent. After verifying that Navitoclax not only successfully selected CRISPR^{+}BCL-XL^{+}-cells but also displayed a better survival rate than flow cytometry, 8 h after lipofection, cells were also treated with Navitoclax. In all the strategies, a single cell sorting and plate duplication were conducted.

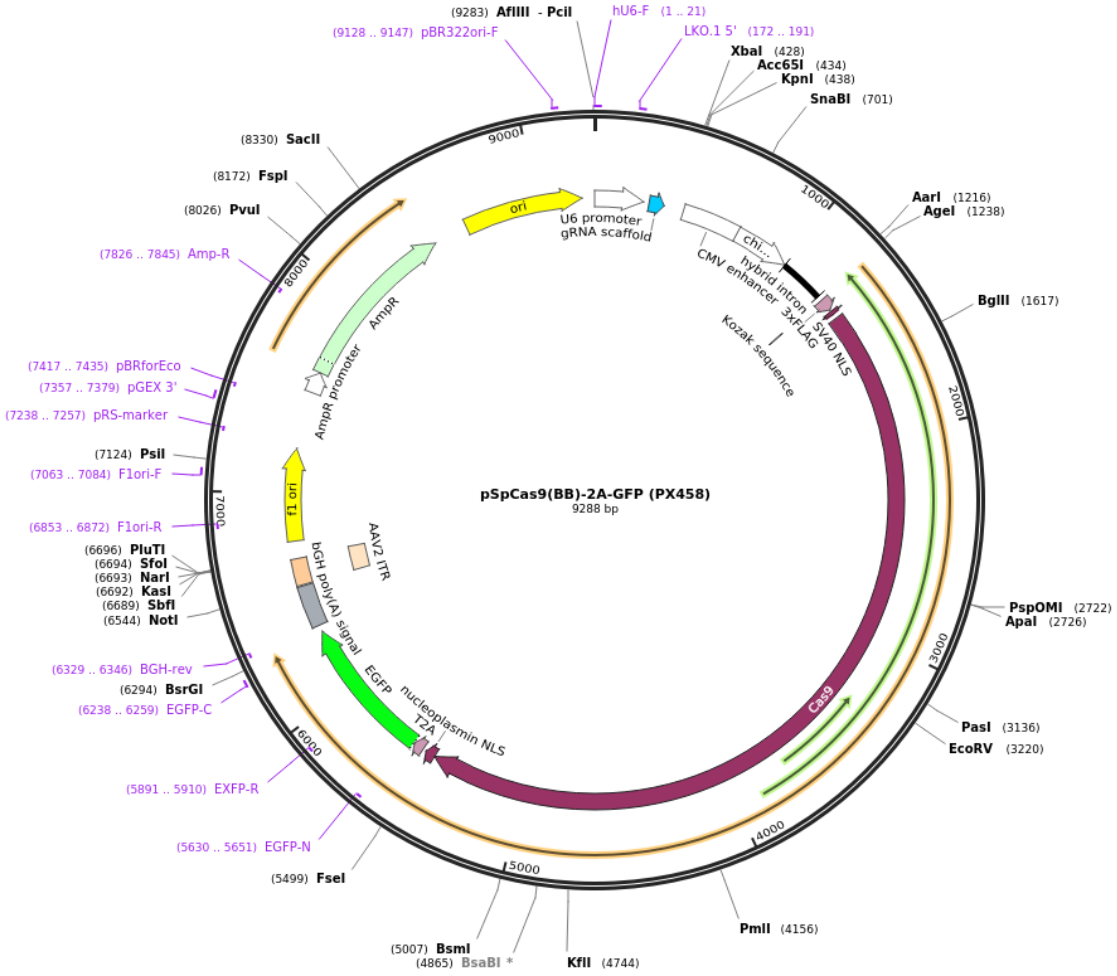

Supplementary Figure S2. The pSpCas9-2A-GFP construct. The guide sequence was cloned into this plasmid by means of restriction enzymes. To confirm a correct cloning of the gRNA construct into the plasmid, the hU6-F primer (5'-GAGGGCCTATTTCCCATGATT-3') was used. The nuclease Cas9 is also incorporated, being unnecessary to use a second vector during transfection. Moreover, it was possible to visualize a successful transfection thanks to the presence of the reporter gene GFP. Image modified from Addgene.

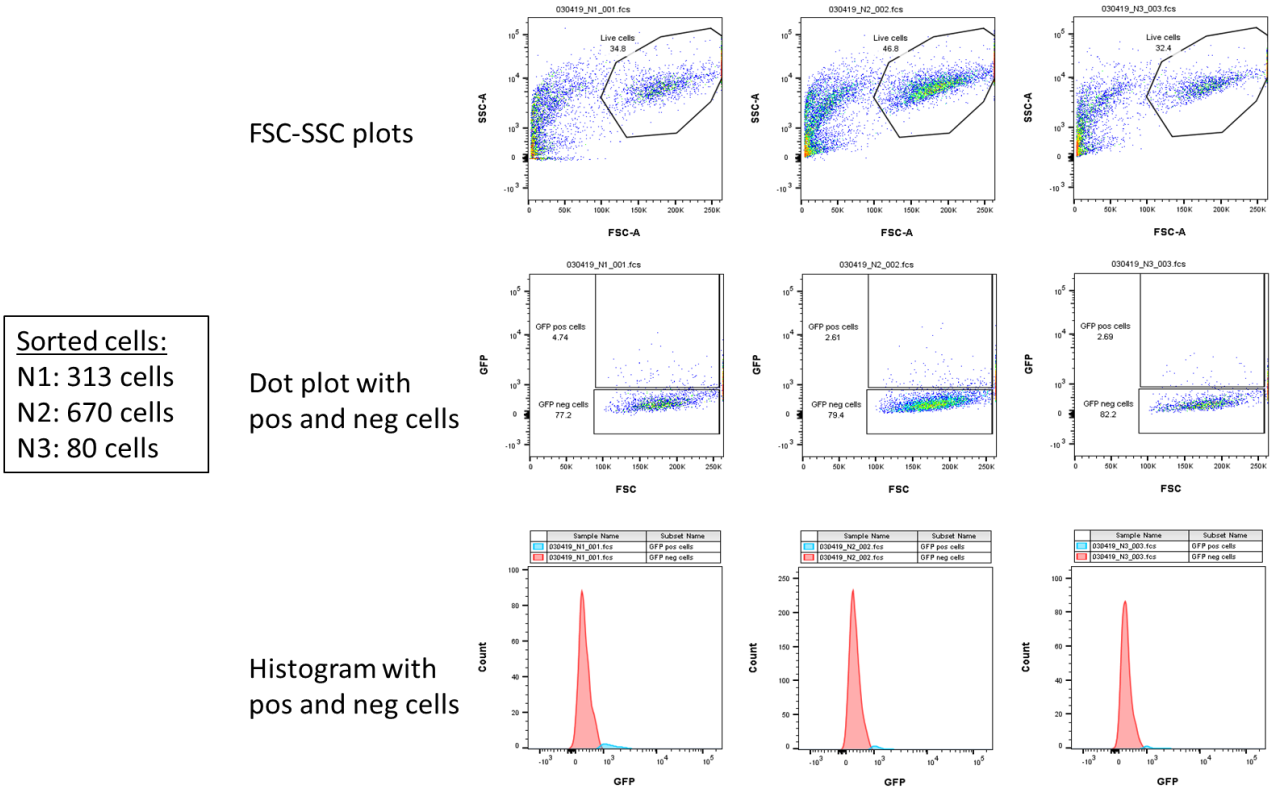

Supplementary Figure S3. Number of transfected cells with different CRISPR plasmids. From the three constructs of gRNA, construct N2 showed better transfection efficacy compared to N1 and N3. GFP^{+} hiPSCs harbouring construct N2 were a total of 670 cells, more than the double harbouring construct N1. Only 80 cells were successfully transfected with construct N3.

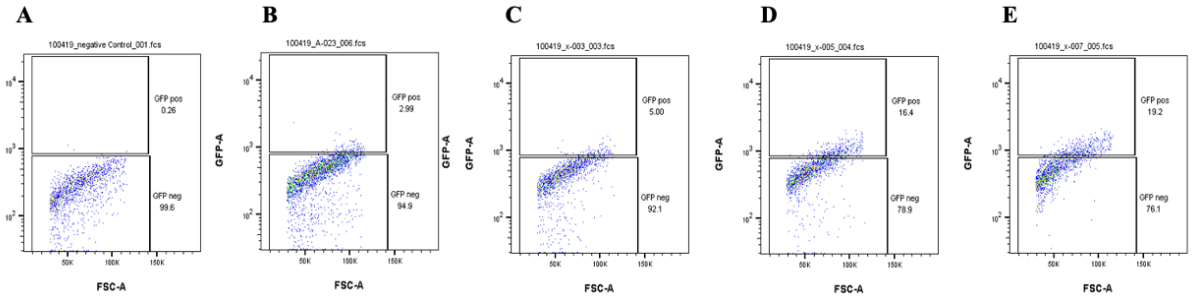

Supplementary Figure S4. Transfection efficiency with different Nucleofactor® programs. Transfected cells were visualized by means of the GFP reporter. (**A**) Negative control with untransfected cells. (**B**) With A-023 Nucleofactor® Program, 2.99 % of the cells were transfected. (**C-E**) Nucleofactor® programs X-003, X-005 and X-007, showed higher transfection efficiencies with 5 %, 16.4 % and 19.2 % positive cells respectively. However, despite performing better, the survival rate with X-003, X-005 and X-007, were extremely low. Therefore, for subsequent electroporations the A-023 Nucleofactor® Program was chosen.

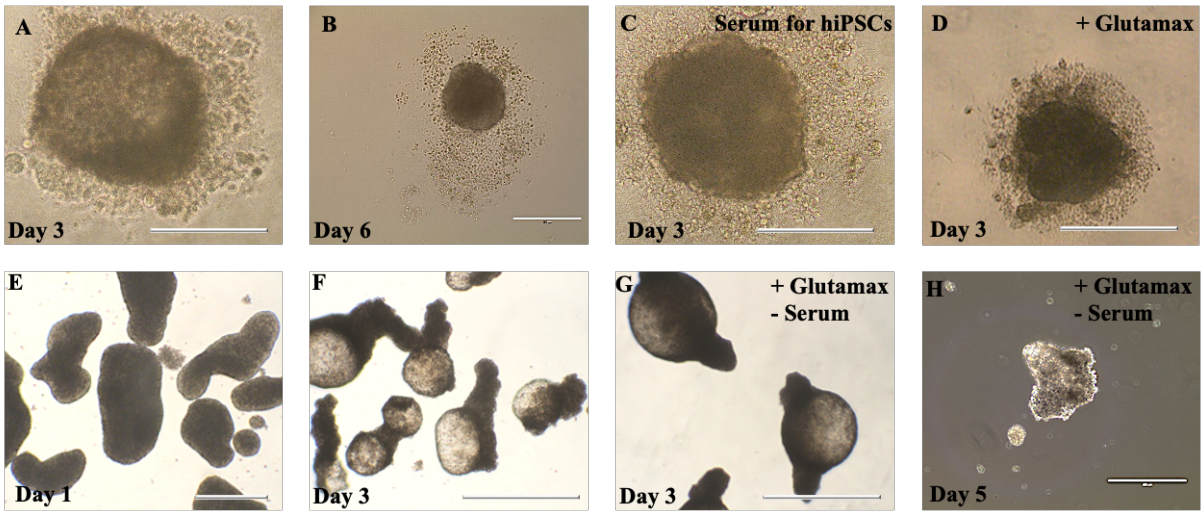

Supplementary Figure S5. Suboptimal EBs. (**A**) Unsuitable EB at day 3 lacking smooth edges and dense center. (**B**) Small-sized EB at day 6 surrounded by a large amount of cell debris and showing irregular edges. (**C**) EB grown in a medium supplemented with FBS compatible with stem cells, and still showing uneven edges. (**D**) EB at day 3 generated from a medium supplemented with Glutamax and lacking optical clearing and smooth edges. (**E-H)** EBs obtained with the methodology described in Hongjun's publication (72). (**E)** Day 1 EBs lacking round shapes and attached to each other. (**F-G)** At day 3, EBs formed bubble-like structures with low cell density. The addition of Glutamax or the absence of the serum in the media did not modify the outcome. (**H**) An example of EB at day 5 lacking smooth surface and of a very small size. Scale bars A, C-D = 200 µm; B, E-H = 400 µm.

A

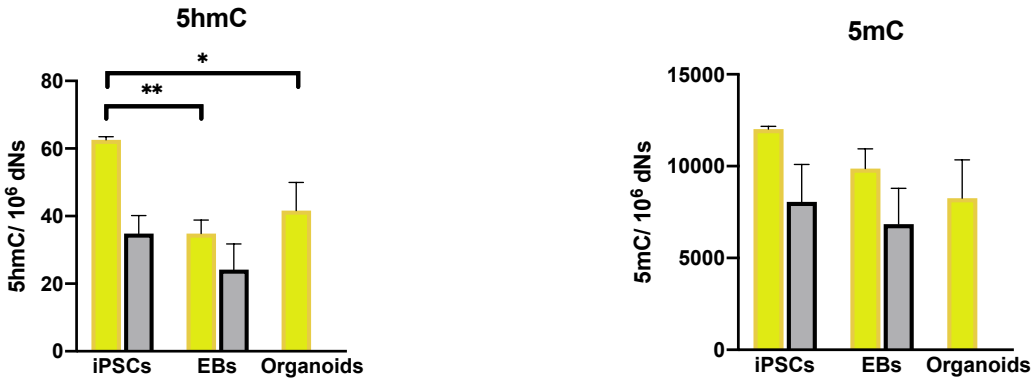

B

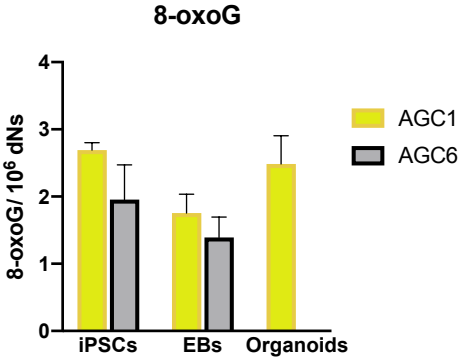

Supplementary Figure S6. Absolute values for 5hmC, 5mC and 8-oxoG in three stages of cerebral organoid development. Since the number of epigenetic modifications and 8-oxoG lesion differed considerably between AGC1 and AGC6, Two-way ANOVA was used to evaluate each clone separately. (**A**) For AGC1, the levels of 5hmC in hiPSCs were significantly higher than those in EBs and organoids. While the trend was similar for AGC6 clone, the difference between stages was not statistically significant. For both clones, there was a slightly decrease in 5mC levels during the organoid development, being hiPSC the stage with a higher number of this modification. (**B**) No significant difference in 8-oxoG levels was found between the stages for any of the two clones analyzed. However, there was a decrease in the amount of 8-oxoG between hiPSCs and EBs. Interestingly, levels increased again in the organoid stage. No data of AGC6-derived organoids is shown since the extracted genomic DNA was insufficient for the measurements with LC-MS.
All data plotted above are numbers of modifications every million nucleotides
Error bar shows the mean ± SEM. A, n= 3; B, n= 3-6 samples per stage. *p<0.05; **p< 0.01.

7.2. Culture Media for Cerebral Organoids Development

1. Medium for EBs

Lancaster medium

Name	ml
DMEM/F12	30
KOSR	7,5
ES-FBS	1,125
MEM-NEAA	0,375
2-ME 50mM	3,5 µl
Y-27632 (20 mM)	150 µl
bFGF (15 ng/ul)	150 ng

Perriot medium

Name	ml
DMEM/F12	30
N2	0.3
B-27 (Without vit A)	0.6
2-ME 50mM	3,5 µl
Y-27632 (10 µM)	30 µl
bFGF (10 ng/mL)	12 µl

2. Neural Induction Medium

Name	ml
DMEM/F12	50
MEM-NEAA	0,5
N2 Supple	0,5
Heparin (5mg/ml)	50 µl

3. Neural Differentiation Medium with and without vitamin A

Name	ml	ml	ml	ml
DMEM/F12	125	12,5	25	200
Neurobasal	125	12,5	25	200
N2 Supple	1,25	125 µl	250 µl	2
MEM-NEAA	1,25	125 µl	250 µl	2
B27 Supple -VitA	2,5	250 µl	0,5	4
B27 Supple +VitA	2,5	250 µl	0,5	4
Insulin	62,5 µl	6,25 µl	12,5 µl	100 µl
2-ME 50mM	87,5 µl	8,75 µl	17,5 µl	140 µl

7.3. Supplementary Tables

Supplementary Table 1. Antibodies for tissue characterization

Name	Host	Cat. no	Dilution	Company
DCX	Rabbit	ab18723	1/1000	Abcam
Tuj1	Mouse	MAB1195	1/1000	R&D Systems
Alexa 594	Goat	A11037	1/500	Thermo Fisher Scientific
Alexa 488	Goat	A11001	1/500	Thermo Fisher Scientific
Nestin	Rabbit	N5413	1/1000	Sigma Aldrich
Pax6	Mouse	MAB5552	1/1000	Sigma Aldrich

Supplementary Table 2. Primer list for qPCR targets

Gene	Forward Primer	Reverse Primer
hOCT-4	GTACTCCTCGGTCCCTTTCC	CAAAAACCCTGGCACAAACT
hNANOG	AATACCTCAGCCTCCAGCAGATG	TGCGTCACACCATTGCTATTCTTC
hDCX	TCAGGGAGTGCGTTACATTTAC	GTTGGGATTGACATTCTTGGTG
hPAX6	GCCCTCACAAACACCTACAG	TCATAACTCCGCCCATTCAC
hNESTIN	GGCGCACCTCAAGATGTCC	CTTGGGGTCCTGAAAGCTG
hß-ACTIN	GTTACAGGAAGTCCCTTGCCATCC	CACCTCCCCTGTGTGGACTTGGG
hTUJ1	GCAACTACGTGGGCGACT	TCGAGGCACGTACTTGTGAG
hMAP2	CAGGAGACAGAGATGAGAATTCC	CAGGAGTGATGGCAGTAGAC
hMUTYH a	GAGGAGCCTCTAGAACTATGA	CTTGGCCTGACTGTTGTTCT
hMUTYHb	CTCCGTGTTCTGCTGTCTTC	CTTGGCCTGACTGTTGTTCT
hOGG1	CTCCAACAACAACATCGCC	GAGATGAGCCTCCACCTCTG

Supplementary Table 3. Hydrolysis master mix for LC-MS

Reagent	Vol. per reaction
0.1 M NH_4Ac pH 6.0	10
0.2 MgCl2	0.5
NP1	0.1
benzonase	0.1
AP	0.25
1 µM IS 8oxoG	1.0
1 µM IS 5hmC	1.0
10 mM BHT	1.2
10 mM DFO	1.2
water	3.6

8. References

1. Magistretti PJ, Allaman I. A cellular perspective on brain energy metabolism and functional imaging. Neuron. 2015;86(4):883-901.
2. Lutz PL, Nilsson GrE, Prentice HM. The brain without oxygen : causes of failure and molecular mechanisms for survival. Dordrecht: Kluwer Academic Publ; 2003.
3. Saver JL. Time is brain--quantified. Stroke. 2006;37(1):263-6.
4. Schieber M, Chandel NS. ROS function in redox signaling and oxidative stress. Curr Biol. 2014;24(10):R453-62.
5. Ray PD, Huang BW, Tsuji Y. Reactive oxygen species (ROS) homeostasis and redox regulation in cellular signaling. Cell Signal. 2012;24(5):981-90.
6. Whitaker AM, Schaich MA, Smith MR, Flynn TS, Freudenthal BD. Base excision repair of oxidative DNA damage: from mechanism to disease. Frontiers in bioscience (Landmark edition). 2017;22:1493-522.
7. Garbarino VR, Orr ME, Rodriguez KA, Buffenstein R. Mechanisms of oxidative stress resistance in the brain: Lessons learned from hypoxia tolerant extremophilic vertebrates. Arch Biochem Biophys. 2015;576:8-16.
8. Lambeth JD. NOX enzymes and the biology of reactive oxygen. Nat Rev Immunol. 2004;4(3):181-9.
9. Dickinson BC, Peltier J, Stone D, Schaffer DV, Chang CJ. Nox2 redox signaling maintains essential cell populations in the brain. Nat Chem Biol. 2011;7(2):106-12.
10. Massaad CA, Klann E. Reactive oxygen species in the regulation of synaptic plasticity and memory. Antioxid Redox Signal. 2011;14(10):2013-54.
11. Bazopoulou D, Knoefler D, Zheng Y, Ulrich K, Oleson BJ, Xie L, et al. Developmental ROS individualizes organismal stress resistance and lifespan. Nature. 2019.
12. Smith CD, Carney JM, Starke-Reed PE, Oliver CN, Stadtman ER, Floyd RA, et al. Excess brain protein oxidation and enzyme dysfunction in normal aging and in Alzheimer disease. Proc Natl Acad Sci U S A. 1991;88(23):10540-3.
13. Olanow CW. Oxidation reactions in Parkinson's disease. Neurology. 1990;40(10 Suppl 3):suppl 32-7; discussion 7-9.
14. Sohal RS, Mockett RJ, Orr WC. Mechanisms of aging: an appraisal of the oxidative stress hypothesis. Free Radic Biol Med. 2002;33(5):575-86.
15. Cobley JN, Fiorello ML, Bailey DM. 13 reasons why the brain is susceptible to oxidative stress. Redox Biol. 2018;15:490-503.
16. Alberts B, Johnson A, Lewis J, Morgan D, Raff MC, Roberts K, et al. Molecular biology of the cell2015.
17. Balestrazzi A, Achary VM, Macovei A, Yoshiyama KO, Sakamoto AN. Editorial: Maintenance of Genome Integrity: DNA Damage Sensing, Signaling, Repair, and Replication in Plants. Front Plant Sci. 2016;7:64.
18. Tubbs A, Nussenzweig A. Endogenous DNA Damage as a Source of Genomic Instability in Cancer. Cell. 2017;168(4):644-56.
19. Radak Z, Boldogh I. 8-Oxo-7,8-dihydroguanine: links to gene expression, aging, and defense against oxidative stress. Free Radic Biol Med. 2010;49(4):587-96.
20. Maki H. Origins of spontaneous mutations: specificity and directionality of base-substitution, frameshift, and sequence-substitution mutageneses. Annu Rev Genet. 2002;36:279-303.

21. Nakabeppu Y, Sakumi K, Sakamoto K, Tsuchimoto D, Tsuzuki T, Nakatsu Y. Mutagenesis and carcinogenesis caused by the oxidation of nucleic acids. Biol Chem. 2006;387(4):373-9.
22. Jacobs AL, Schär P. DNA glycosylases: in DNA repair and beyond. Chromosoma. 2012;121(1):1-20.
23. Krokan HE, Standal R, Slupphaug G. DNA glycosylases in the base excision repair of DNA. Biochem J. 1997;325 (Pt 1)(Pt 1):1-16.
24. Markkanen E, Dorn J, Hübscher U. MUTYH DNA glycosylase: the rationale for removing undamaged bases from the DNA. Front Genet. 2013;4:18.
25. Bjørås KØ, Sousa Mirta ML, Sharma A, Fonseca DM, Søgaard CK, Bjørås M, et al. Monitoring of the spatial and temporal dynamics of BER/SSBR pathway proteins, including MYH, UNG2, MPG, NTH1 and NEIL1-3, during DNA replication. Nucleic Acids Research. 2017;45(14):8291-301.
26. Liu P, Qian L, Sung JS, de Souza-Pinto NC, Zheng L, Bogenhagen DF, et al. Removal of oxidative DNA damage via FEN1-dependent long-patch base excision repair in human cell mitochondria. Mol Cell Biol. 2008;28(16):4975-87.
27. Dallosso AR, Dolwani S, Jones N, Jones S, Colley J, Maynard J, et al. Inherited predisposition to colorectal adenomas caused by multiple rare alleles of MUTYH but not OGG1, NUDT1, NTH1 or NEIL 1, 2 or 3. Gut. 2008;57(9):1252-5.
28. Russo MT, De Luca G, Degan P, Parlanti E, Dogliotti E, Barnes DE, et al. Accumulation of the oxidative base lesion 8-hydroxyguanine in DNA of tumor-prone mice defective in both the Myh and Ogg1 DNA glycosylases. Cancer Res. 2004;64(13):4411-4.
29. Larsen E, Reite K, Nesse G, Gran C, Seeberg E, Klungland A. Repair and mutagenesis at oxidized DNA lesions in the developing brain of wild-type and Ogg1-/- mice. Oncogene. 2006;25(17):2425-32.
30. Zarakowska E, Gackowski D, Foksinski M, Olinski R. Are 8-oxoguanine (8-oxoGua) and 5-hydroxymethyluracil (5-hmUra) oxidatively damaged DNA bases or transcription (epigenetic) marks? Mutat Res Genet Toxicol Environ Mutagen. 2014;764-765:58-63.
31. Maltseva DV, Baykov AA, Jeltsch A, Gromova ES. Impact of 7,8-dihydro-8-oxoguanine on methylation of the CpG site by Dnmt3a. Biochemistry. 2009;48(6):1361-8.
32. Zhou X, Zhuang Z, Wang W, He L, Wu H, Cao Y, et al. OGG1 is essential in oxidative stress induced DNA demethylation. Cell Signal. 2016;28(9):1163-71.
33. Spruijt CG, Gnerlich F, Smits AH, Pfaffeneder T, Jansen PW, Bauer C, et al. Dynamic readers for 5-(hydroxy)methylcytosine and its oxidized derivatives. Cell. 2013;152(5):1146-59.
34. Bjorge MD, Hildrestrand GA, Scheffler K, Suganthan R, Rolseth V, Kusnierczyk A, et al. Synergistic Actions of Ogg1 and Mutyh DNA Glycosylases Modulate Anxiety-like Behavior in Mice. Cell Rep. 2015;13(12):2671-8.
35. Xia L, Huang W, Bellani M, Seidman MM, Wu K, Fan D, et al. CHD4 Has Oncogenic Functions in Initiating and Maintaining Epigenetic Suppression of Multiple Tumor Suppressor Genes. Cancer Cell. 2017;31(5):653-68.e7.
36. Wang R, Hao W, Pan L, Boldogh I, Ba X. The roles of base excision repair enzyme OGG1 in gene expression. Cell Mol Life Sci. 2018;75(20):3741-50.
37. Hao W, Qi T, Pan L, Wang R, Zhu B, Aguilera-Aguirre L, et al. Effects of the stimuli-dependent enrichment of 8-oxoguanine DNA glycosylase1 on chromatinized DNA. Redox Biol. 2018;18:43-53.

38. Liu D, Croteau DL, Souza-Pinto N, Pitta M, Tian J, Wu C, et al. Evidence that OGG1 glycosylase protects neurons against oxidative DNA damage and cell death under ischemic conditions. J Cereb Blood Flow Metab. 2011;31(2):680-92.
39. Cho J, Yu NK, Choi JH, Sim SE, Kang SJ, Kwak C, et al. Multiple repressive mechanisms in the hippocampus during memory formation. Science. 2015;350(6256):82-7.
40. Stocum DL. Amphibian regeneration and stem cells. Curr Top Microbiol Immunol. 2004;280:1-70.
41. Chagastelles PC, Nardi NB. Biology of stem cells: an overview. Kidney Int Suppl (2011). 2011;1(3):63-7.
42. Aranda-Anzaldo A. The post-mitotic state in neurons correlates with a stable nuclear higher-order structure. Commun Integr Biol. 2012;5(2):134-9.
43. Takahashi K, Yamanaka S. Induction of pluripotent stem cells from mouse embryonic and adult fibroblast cultures by defined factors. Cell. 2006;126(4):663-76.
44. Yu J, Vodyanik MA, Smuga-Otto K, Antosiewicz-Bourget J, Frane JL, Tian S, et al. Induced pluripotent stem cell lines derived from human somatic cells. Science. 2007;318(5858):1917-20.
45. Park IH, Zhao R, West JA, Yabuuchi A, Huo H, Ince TA, et al. Reprogramming of human somatic cells to pluripotency with defined factors. Nature. 2008;451(7175):141-6.
46. Takahashi K, Tanabe K, Ohnuki M, Narita M, Ichisaka T, Tomoda K, et al. Induction of pluripotent stem cells from adult human fibroblasts by defined factors. Cell. 2007;131(5):861-72.
47. Kelava I, Lancaster MA. Stem Cell Models of Human Brain Development. Cell stem cell. 2016;18(6):736-48.
48. Park IH, Lerou PH, Zhao R, Huo H, Daley GQ. Generation of human-induced pluripotent stem cells. Nat Protoc. 2008;3(7):1180-6.
49. Sterneckert JL, Reinhardt P, Schöler HR. Investigating human disease using stem cell models. Nature Reviews Genetics. 2014;15:625.
50. Bock C, Kiskinis E, Verstappen G, Gu H, Boulting G, Smith ZD, et al. Reference Maps of human ES and iPS cell variation enable high-throughput characterization of pluripotent cell lines. Cell. 2011;144(3):439-52.
51. Heyer WD, Ehmsen KT, Liu J. Regulation of homologous recombination in eukaryotes. Annu Rev Genet. 2010;44:113-39.
52. Hendriks WT, Warren CR, Cowan CA. Genome Editing in Human Pluripotent Stem Cells: Approaches, Pitfalls, and Solutions. Cell Stem Cell. 2016;18(1):53-65.
53. Jinek M, Chylinski K, Fonfara I, Hauer M, Doudna JA, Charpentier E. A programmable dual-RNA-guided DNA endonuclease in adaptive bacterial immunity. Science. 2012;337(6096):816-21.
54. Ding Q, Regan SN, Xia Y, Oostrom LA, Cowan CA, Musunuru K. Enhanced efficiency of human pluripotent stem cell genome editing through replacing TALENs with CRISPRs. Cell Stem Cell. 2013;12(4):393-4.
55. Yang L, Guell M, Byrne S, Yang JL, De Los Angeles A, Mali P, et al. Optimization of scarless human stem cell genome editing. Nucleic Acids Res. 2013;41(19):9049-61.
56. Cong L, Ran FA, Cox D, Lin S, Barretto R, Habib N, et al. Multiplex genome engineering using CRISPR/Cas systems. Science. 2013;339(6121):819-23.
57. Lancaster MA, Knoblich JA. Generation of cerebral organoids from human pluripotent stem cells. Nat Protoc. 2014;9(10):2329-40.

58. Stiles J, Jernigan TL. The basics of brain development. Neuropsychol Rev. 2010;20(4):327-48.
59. Barresi MJF, Gilbert SF. Developmental biology2020.
60. Evans M. Discovering pluripotency: 30 years of mouse embryonic stem cells. Nat Rev Mol Cell Biol. 2011;12(10):680-6.
61. Bystron I, Blakemore C, Rakic P. Development of the human cerebral cortex: Boulder Committee revisited. Nat Rev Neurosci. 2008;9(2):110-22.
62. Evsyukova I, Plestant C, Anton ES. Integrative mechanisms of oriented neuronal migration in the developing brain. Annu Rev Cell Dev Biol. 2013;29:299-353.
63. Sur M, Leamey CA. Development and plasticity of cortical areas and networks. Nat Rev Neurosci. 2001;2(4):251-62.
64. Zhang SC, Wernig M, Duncan ID, Brustle O, Thomson JA. In vitro differentiation of transplantable neural precursors from human embryonic stem cells. Nat Biotechnol. 2001;19(12):1129-33.
65. Garitaonandia I, Amir H, Boscolo FS, Wambua GK, Schultheisz HL, Sabatini K, et al. Increased risk of genetic and epigenetic instability in human embryonic stem cells associated with specific culture conditions. PLoS One. 2015;10(2):e0118307.
66. Grobarczyk B, Franco B, Hanon K, Malgrange B. Generation of Isogenic Human iPS Cell Line Precisely Corrected by Genome Editing Using the CRISPR/Cas9 System. Stem Cell Rev Rep. 2015;11(5):774-87.
67. Lin YT, Seo J, Gao F, Feldman HM, Wen HL, Penney J, et al. APOE4 Causes Widespread Molecular and Cellular Alterations Associated with Alzheimer's Disease Phenotypes in Human iPSC-Derived Brain Cell Types. Neuron. 2018;98(6):1294.
68. Li X-L, Li G-H, Fu J, Fu Y-W, Zhang L, Chen W, et al. Highly efficient genome editing via CRISPR–Cas9 in human pluripotent stem cells is achieved by transient BCL-XL overexpression. Nucleic Acids Research. 2018;46(19):10195-215.
69. Perriot S, Mathias A, Perriard G, Canales M, Jonkmans N, Merienne N, et al. Human Induced Pluripotent Stem Cell-Derived Astrocytes Are Differentially Activated by Multiple Sclerosis-Associated Cytokines. Stem Cell Reports. 2018;11(5):1199-210.
70. Qian X, Jacob F, Song MM, Nguyen HN, Song H, Ming G-l. Generation of human brain region–specific organoids using a miniaturized spinning bioreactor. Nature Protocols. 2018;13:565.
71. Chen YH, Pruett-Miller SM. Improving single-cell cloning workflow for gene editing in human pluripotent stem cells. Stem Cell Res. 2018;31:186-92.
72. Watanabe K, Ueno M, Kamiya D, Nishiyama A, Matsumura M, Wataya T, et al. A ROCK inhibitor permits survival of dissociated human embryonic stem cells. Nature biotechnology. 2007;25(6):681-6.
73. Shi J, Wei L. Rho kinase in the regulation of cell death and survival. Arch Immunol Ther Exp (Warsz). 2007;55(2):61-75.
74. Wong M, Tan N, Zha J, Peale FV, Yue P, Fairbrother WJ, et al. Navitoclax (ABT-263) reduces Bcl-x(L)-mediated chemoresistance in ovarian cancer models. Mol Cancer Ther. 2012;11(4):1026-35.
75. Zeineddine D, Hammoud AA, Mortada M, Boeuf H. The Oct4 protein: more than a magic stemness marker. Am J Stem Cells. 2014;3(2):74-82.
76. Gawlik-Rzemieniewska N, Bednarek I. The role of NANOG transcriptional factor in the development of malignant phenotype of cancer cells. Cancer Biol Ther. 2016;17(1):1-10.

77. Barry D, McDermott K. Differentiation of radial glia from radial precursor cells and transformation into astrocytes in the developing rat spinal cord. Glia. 2005;50(3):187-97.
78. Suter DM, Tirefort D, Julien S, Krause KH. A Sox1 to Pax6 switch drives neuroectoderm to radial glia progression during differentiation of mouse embryonic stem cells. Stem Cells. 2009;27(1):49-58.
79. Zhang J, Jiao J. Molecular Biomarkers for Embryonic and Adult Neural Stem Cell and Neurogenesis. Biomed Res Int. 2015;2015:727542.
80. Soltani MH, Pichardo R, Song Z, Sangha N, Camacho F, Satyamoorthy K, et al. Microtubule-associated protein 2, a marker of neuronal differentiation, induces mitotic defects, inhibits growth of melanoma cells, and predicts metastatic potential of cutaneous melanoma. Am J Pathol. 2005;166(6):1841-50.
81. Karzbrun E, Reiner O. Brain Organoids-A Bottom-Up Approach for Studying Human Neurodevelopment. Bioengineering (Basel). 2019;6(1).
82. Geisert EE, Jr., Frankfurter A. The neuronal response to injury as visualized by immunostaining of class III beta-tubulin in the rat. Neurosci Lett. 1989;102(2-3):137-41.
83. Suzuki S, Namiki J, Shibata S, Mastuzaki Y, Okano H. The neural stem/progenitor cell marker nestin is expressed in proliferative endothelial cells, but not in mature vasculature. J Histochem Cytochem. 2010;58(8):721-30.
84. Ayanlaja AA, Xiong Y, Gao Y, Ji G, Tang C, Abdikani Abdullah Z, et al. Distinct Features of Doublecortin as a Marker of Neuronal Migration and Its Implications in Cancer Cell Mobility. Front Mol Neurosci. 2017;10:199.
85. Barnham KJ, Masters CL, Bush AI. Neurodegenerative diseases and oxidative stress. Nat Rev Drug Discov. 2004;3(3):205-14.
86. Scheffler K, Bjoras KO, Bjoras M. Diverse functions of DNA glycosylases processing oxidative base lesions in brain. DNA Repair (Amst). 2019;81:102665.
87. Wang H. Modeling Neurological Diseases With Human Brain Organoids. Front Synaptic Neurosci. 2018;10:15.
88. Otani T, Marchetto MC, Gage FH, Simons BD, Livesey FJ. 2D and 3D Stem Cell Models of Primate Cortical Development Identify Species-Specific Differences in Progenitor Behavior Contributing to Brain Size. Cell Stem Cell. 2016;18(4):467-80.
89. de Souza N. Organoid variability examined. Nature Methods. 2017;14(7):655-.
90. Xie AW, Binder BYK, Khalil AS, Schmitt SK, Johnson HJ, Zacharias NA, et al. Controlled Self-assembly of Stem Cell Aggregates Instructs Pluripotency and Lineage Bias. Scientific Reports. 2017;7(1):14070.
91. Ferguson R, Subramanian V. Embryoid body arrays: Parallel cryosectioning of spheroid/embryoid body samples for medium through-put analysis. Stem Cell Res. 2018;28:125-30.
92. Watanabe M, Buth JE, Vishlaghi N, de la Torre-Ubieta L, Taxidis J, Khakh BS, et al. Self-Organized Cerebral Organoids with Human-Specific Features Predict Effective Drugs to Combat Zika Virus Infection. Cell Rep. 2017;21(2):517-32.
93. Yakoub AM, Sadek M. Development and Characterization of Human Cerebral Organoids: An Optimized Protocol. Cell Transplant. 2018;27(3):393-406.
94. Yakoub AM. Cerebral organoids exhibit mature neurons and astrocytes and recapitulate electrophysiological activity of the human brain. Neural Regen Res. 2019;14(5):757-61.

95. Vinci L, Ravarino A, Fanos V, Naccarato AG, Senes G, Gerosa C, et al. Immunohistochemical markers of neural progenitor cells in the early embryonic human cerebral cortex. Eur J Histochem. 2016;60(1):2563.
96. Menezes JR, Luskin MB. Expression of neuron-specific tubulin defines a novel population in the proliferative layers of the developing telencephalon. J Neurosci. 1994;14(9):5399-416.
97. Gu A, Ji G, Yan L, Zhou Y. The 8-oxoguanine DNA glycosylase 1 (ogg1) decreases the vulnerability of the developing brain to DNA damage. DNA Repair (Amst). 2013;12(12):1094-104.
98. Luo C, Lancaster MA, Castanon R, Nery JR, Knoblich JA, Ecker JR. Cerebral Organoids Recapitulate Epigenomic Signatures of the Human Fetal Brain. Cell Rep. 2016;17(12):3369-84.
99. Fleming AM, Ding Y, Burrows CJ. Oxidative DNA damage is epigenetic by regulating gene transcription via base excision repair. Proc Natl Acad Sci U S A. 2017;114(10):2604-9.

NTNU

Norwegian University of
Science and Technology